Zhang, Y., Oliver, T. A. A., Das, S., Roy, A., Ashfold, M. N. R., & Bradforth, S. E. (2013). Exploring the energy disposal immediately after bond-breaking in solution: the wavelength-dependent excited state dissociation pathways of para-methylthiophenol. *Journal of Physical Chemistry A*, *117*(46), 12125-12137. https://doi.org/10.1021/jp405160n

Exploring the Energy Disposal Immediately After Bond-Breaking in Solution: the Wavelength-Dependent Excited State Dissociation Pathways of *para*-Methylthiophenol

Yuyuan Zhang,[1‡§] Thomas A.A. Oliver,[2#§] Saptaparna Das,[1] Anirban Roy,[1] Michael N.R. Ashfold[2] and Stephen E. Bradforth[1*]

[1]Department of Chemistry, University of Southern California, Los Angeles, CA 90089-0482, USA

[2]School of Chemistry, Cantocks Close, University of Bristol, BS8 1TS, UK

Keywords: conical intersections, solution reaction dynamics, ultrafast photodissociation, radical recombination.

[§] These authors contributed equally to this work

[‡] Present address: Department of Chemistry and Biochemistry, Montana State University, Bozeman, MT 59717, USA

[#] Present address: Department of Chemistry, University of California, Berkeley, CA 94720, USA

* stephen.bradforth@usc.edu, Tel: (213) 740-0461. Fax: (213) 740-3972

Abstract

A wavelength-resolved (λ_{pump} = 295, 285, 270 and 267 nm) photodissociation study of *para*-methylthiophenol (*p*-MePhSH) in ethanol solution has been performed using femtosecond transient absorption (TA) spectroscopy and the results compared with those from studies of the corresponding photodissociation in cyclohexane solution at 270 nm. Anisotropy spectra are used to identify the electronic character of the initially populated excited state(s). S–H bond fission is found to occur *via* the dissociative $S_2(1^1\pi\sigma^*)$ state, which can be populated directly, or by ultrafast non-radiative transitions from the $S_3(2^1\pi\pi^*)$ state, or by very efficient tunneling from the $S_1(1^1\pi\pi^*)$ state, depending on the excitation wavelength – in line with conclusions from previous gas-phase studies of this same molecular photodissociation (Oliver, T.A.A.; King, G.A.; Tew, D.P.; Dixon R.N.; Ashfold, M.N.R. *J. Phys. Chem. A* **2012**, *116* 12444). *p*-MePhS radicals are observed on a timescale faster than the instrument response at all wavelengths, but the available time resolution affords a rare opportunity to explore the branching between different electronic states of a product (the $\tilde{A}$ and $\tilde{X}$ states of the *p*-MePhS radical in this case). The present study provides estimates of this branching in the products formed immediately after first pass through the conical intersection (CI) between the S_2 and S_0 states. At 270 nm, for example, we identify a marked population inversion in the radical products, in contrast to the reported gas phase behavior. The finding that the contrast in branching ratio is largest between cyclohexane solution and the gas phase, with ethanol being intermediate, can be rationalized by recognizing the differing distributions of the S–H torsion angle (relative to the ring plane) in a room temperature solution compared with in a jet-cooled molecular beam. The available time resolution also allows exploration of the electronic quenching of nascent $\tilde{A}$ state radicals as solvent motion encourages re-crossing of the S_2/S_0 CI. The average separation distance, $\langle r_0 \rangle$, between the H + *p*-MePhS products arising in successful dissociation events is seen to increase

with decreasing photolysis wavelength. This finding accords with the previous gas phase results, which determined that most of the excess energy following population of the dissociative S_2 state (directly, or by ultrafast coupling from the S_3 state) is released as product translation, and the expectation that $\langle r_0 \rangle$ should scale with the total kinetic energy release. The present work also confirms that geminate recombination of the H + *p*-MePhS products leads not just to reformation of parent *p*-MePhSH molecules but also to alternative adducts wherein the H atom bonds to the benzene ring. Analysis of the present data and results of high level *ab initio* calculations together with recent UV-IR pump-probe measurements (Murdock, D.; Harris, S.J.; Karsili, T.N.V.; Greetham, G.M.; Clark, I.P.; Towrie, M.; Orr-Ewing, A.J.; Ashfold, M.N.R. *J. Phys. Chem. Lett.* **2012**, 3, 3715) allows identification of the likely adduct structures.

I. Introduction

The role of $n\sigma^*$ and $\pi\sigma^*$ states has attracted much attention in excited state chemical dynamics over the past decade.[1-3] These excited states are formed by promotion of an electron from a non-bonding *n* orbital, or a bonding π orbital, to an anti-bonding σ^* orbital. $(n/\pi)\sigma^*$ states are recognized as essential for driving most excited state photofragmentation mechanisms, for example X–H (X = N, O, S) bond breaking in H_2O,[4] NH_3 [5,6] and in various heteroaromatic molecules,[1] many of which serve as the building blocks of biomolecules. By monitoring the kinetic energy of a hydrogen atom photofragment, gas phase experiments are able to provide intricate details of X–H bond fission dynamics. For example, Wittig and co-workers have determined that upon photoexcitation of methanol to its first $n\sigma^*$ state, O–H bond fission occurs in < 1 ps as inferred from recoil anisotropy, generating $CH_3O(\tilde{X})$ radicals with a modest amount of vibrational excitation and that most of the photon energy over and above that required to cleave the O–H bond is partitioned into H atom translation.[7]

In the solution phase, there are many new dynamical complexities. For example, solvation can shift the potential energy curves (PECs) and introduce caging.[8] Differential shifts of the PECs induced by solvation and solvent fluctuations that modulate the local electrostatics can respectively affect the location of, and how flux approaches, a curve crossing.[9] As the curve crossing is a point of branching into different product channels, these environmental effects can entirely change the ensuing dynamics in solution relative to the gas phase.[10,11] Caging refers to an ultrafast process where the dissociating molecule encounters the first solvent layer and there is a non-negligible probability for the ejected fragment to recoil rather than punch its way out, shortening the bond that was just broken. One outcome is immediate recombination to reform the parent molecule, or an isomer thereof.[12-,14] Caging can also return the molecule to the region of curve-crossing for a second time, allowing a renewed possibility of branching. This possibility is often responsible for rapid quenching of electronically excited state products in the solution phase, thus depriving us of observing the initial electronic branching – one of the mainstay observables in gas phase reaction dynamics (see for example ref. 5).

Consider an example of aromatic $\pi\sigma^*$ reactivity,[1] the photodissociation of *para*-methylthiophenol, *p*-MePhS–H.[15-17] Fig. 1 shows the PECs of the *isolated p*-MePhSH molecule

for the ground and first three excited singlet and triplet states as a function of the S–H stretch coordinate. The states are labeled according to their diabatic character and in ascending order of energy in the vFC region. The S_2 and T_3 states are formed by $\sigma^*\leftarrow\pi$ excitation, whereas the S_1, S_3 T_1 and T_2 states are formed by $\pi^*\leftarrow\pi$ excitation. Because of the spin-orbit coupling introduced by the sulfur, it is plausible that initial excited singlet states can couple to lower lying triplet states, as supported by recent finding of ultrafast intersystem crossing (ISC) in 6-thioguanosine.[18,19] Photofragment translational spectroscopy (HRA-PTS) studies have clearly shown that H + *para*-methylthiophenoxyl (*p*-MePhS) in its electronic $\tilde{A}$ state is one of the product channels populated following photoexcitation from the *p*-MePhSH ground (S_0) state. The branching between the H + *p*-MePhS($\tilde{X}$) and H + *p*-MePhS($\tilde{A}$) product channels occurs at the S_2/S_0 conical intersection (CI) and is strongly dependent on pump wavelength.[15,20-22] It was observed that between 295–271 nm, vibrational levels of the S_1 state were initially photo-prepared, dissociating rapidly *via* tunneling through the barrier under the S_1/S_2 CI[15] (see Fig. 1). This proposed mechanism is very similar to that recently identified for phenol in a collision-free environment.[23,24] The absorption cross-section for direct excitation to the $^1\pi\sigma^*$ state increases at $\lambda < 271$ nm, and by 260 nm it becomes the only state populated in the photo-excitation.[15]

Our earlier transient absorption work on this system in ethanol and cyclohexane solution[16,17] has shown that for photolysis at a few excitation wavelengths (270, 267 and 200 nm), S–H bond fission driven *via* the lowest excited $^1\pi\sigma^*$ potential energy surface (PES) is active just as in the gas phase, promptly producing H + *p*-MePhS radicals. This work also suggested that caging of H atoms emerging at the $\tilde{A}$ state asymptote followed by re-crossing at the $S_2(^1\pi\sigma^*)/S_0$ CI led to electronic deactivation to *p*-MePhS($\tilde{X}$) radicals.[16,17] This sequence of events is likely complete within the duration of even a typical ultrashort UV laser pulse (100 – 150 fs). Compounding this, within the delay range where the pump and probe pulses overlap, pump-probe signals corresponding to the nascent products are be expected to overlap with an often-times large coherent 2-photon absorption (2PA) signal. In light of these factors, *p*-MePhS($\tilde{A}$) radicals were considered sufficiently short-lived to preclude detection; this in turn hindered our ability to consider how the dissociating molecule encounters the $S_2(^1\pi\sigma^*)/S_0$ CI on its first pass.

In this paper we have taken a similar approach to the most recent gas phase experiments for this system.[15] Namely, by varying the excitation wavelength we can explore whether the rich excitation-dependent behavior identified for the isolated molecule (*i.e.*, a switch in dissociation mechanism across the 290–267 nm wavelength range [15]) maps into the condensed phase. We use multiple excitation wavelengths: λ_{pump} = 267, 270, 285 and 295 nm and anisotropy measurements to elucidate the initially photo-prepared state of the *p*-MePhSH. The pump wavelength dependence turns out to allow us to differentiate any coherent 2PA signal from that arising from formation of *p*-MePhS($\tilde{A}$)at very early delay times, something that was elusive in earlier work. This resulting electronic branching now gives us a parameter through which we can observe how the solvent modulates the non-adiabatic coupling at the S_2/S_0 CI.

At longer delay times (t > ~5 ps), we have previously seen that the TA band associated with the *p*-MePhS($\tilde{X}$) radical products diminishes in intensity due to diffusive geminate recombination with the H co-fragment.[16,17] Recent 267 nm pump, mid-IR probe measurements have also explored the recombination dynamics after photolysis of *p*-MePhSH in acetonitrile and cyclohexane.[25,26] Infra-red probing provides direct and complementary kinetic information regarding the ground state bleach recovery and the vibrational cooling of the radical. In the current study, we can now examine how the recombination dynamics differs at different photolysis wavelengths. By using standard models for diffusive geminate recombination, [27] we can extract the ejection length of the H-atom, and thereby compare it to the translational kinetic energy release in the unimpeded gas-phase photofragmentation dynamics. As we have noted previously, there are two possible fates for the geminate radical partners that diffusively re-counter each other: either to reform the dissociated S–H bond and yield ground state *p*-MePhSH molecules, or the H atom could recombine with the *p*-MePhS ring to form an adduct.[16,17] In this work, the identity of this adduct is investigated with high level *ab initio* calculations and careful consideration of both the TA and UV-IR pump-probe data. [25,26]

II. Experimental and Theoretical Methods

The TA experiments at USC were achieved by exciting the *p*-MePhSH solution with deep UV pulses (267 – 295 nm) and probing the transient species with a broadband super continuum pulse (typically 310 ≤ λ_{probe} ≤ 650 nm). The 270 nm pump pulses were generated *via* four-wave

mixing of the fundamental 800 nm pulses (30 fs, 32 nm bandwidth, 1 kHz, Coherent Legend) and its second harmonic 400 nm in an Argon-filled hollow-core fiber. The resulting pulses had a bandwidth of 5 nm, and were compressed to 40 ± 5 fs (FWHM as determined by autocorrelation) by a pair of Gires-Tournois interferometer dispersion mirrors.[28] The 267 nm pump pulses was obtained from sum-frequency mixing of 800 nm and 400 nm in a type-II BBO crystal, and a bandwidth of 2 nm and pulse width of 100 fs were obtained. The 285 and 295 nm pump pulses were generated by sum-frequency mixing and subsequent frequency-doubling the output from a two-stage optical parametric amplifier using a type-II phase matching process (OPA-800C, Spectra-Physics). The pre-requisite 570 nm and 590 nm pulses were generated by mixing the 800 nm fundamental with the idler pulse from the OPA in a type-I BBO crystal. The visible output was subsequently frequency-doubled to obtain the desired UV pulse, which in both cases had a 3.2–3.8 nm bandwidth and 100 fs pulse duration as determined by cross-correlation. All experiments employed pulse energies in the range 0.4–1.2 μJ and spot sizes between 100–250 μm (FWHM). TA signals from ethanol solvent were negligible under these experimental conditions. Our previous studies established that all TA signals from the solute *p*-MePhSH varied linearly with pump laser fluence over the range of pulse energies used in this study.[16] In the case of cyclohexane, the solvent gave a non-negligible amount of TA signal which spans the whole probing region.[17]

The broadband supercontinuum probe pulse was generated by focusing a small portion of the 800 nm fundamental into a rotating CaF_2 disk. The relative pump–probe pulse polarization was controlled by rotating the electric field vector of the 800 nm fundamental used to generate the super continuum light *via* a zero-order half waveplate. The polarization purity of the continuum was determined to be >150:1 across the whole probe range (310 – 650 nm), and that of the pump pulses >100:1, as measured by the extinction of the light through a calcite polarizer. Anisotropy spectra were constructed from TA spectra recorded sequentially with parallel and perpendicular polarizations; analysis of such spectra recorded at different time delays provides one route to investigate the time dependence of the product anisotropy. The decay of product anisotropy at selected wavelengths was determined from simultaneously acquired parallel and perpendicular TA signals. This was achieved by rotating the supercontinuum probe polarization by 45° with respect to that of the UV pump pulse. Then using an interference filter after the pulses have

interacted with the sample to select the desired wavelengths (typically with a bandwidth of 10 nm), the *s*- and *p*- components are spatially separated by a Wollaston prism and focused onto different parts of the same 256-pixel photodiode array. The anisotropy ($R(t)$) was calculated from eqn. (1)

$$R(t) = \frac{\Delta A_{\parallel} - \Delta A_{\perp}}{\Delta A_{\parallel} + 2\Delta A_{\perp}}, \quad (1)$$

where $\Delta A_{\parallel}(t)$ and $\Delta A_{\perp}(t)$ represent TA signals recorded at time t with polarization of the pump and probe pulses aligned parallel and perpendicular with respect to each other. All TA experiments employed a wire-guided gravity jet to deliver *p*-MePhSH solutions with a linear flow rate of 1 mm ms^{-1}, ensuring that successive laser shots (1 ms time separation) interrogated a fresh sample.[29] 45 mM and 90 mM concentrations of *p*-MePhSH (97%, TCI America) were used in ethanol (200 Proof, Koptec) and cyclohexane (> 99.99%, spectrophotometric grade, EMD) without further purification. The static absorption spectra of *p*-MePhSH in ethanol and cyclohexane (at 1.5 mM) were measured in a Cary 50 UV-Visible spectrophotometer (Varian), and the static emission spectra were measured in a Fluoromax-3 spectrofluorimeter (Horiba).

Ab initio calculations were performed to assist in identifying the structure and properties of an adduct formed by recombination of the H and *p*-MePhS radicals present in our data.[16,17] Three possible structures were considered; C–H bond formation with one of the benzene ring carbon atoms, in either the *ortho*-, *meta*- or *para*- (*o*-, *m*-, *p*-) positions relative to the C–S bond. We henceforth refer to these as structures A, B and C. The three structures were optimized using Møller-Plesset second order perturbation theory (MP2). To ensure proper convergence, the optimization routine required that the gradient on all the atoms was $< 1 \times 10^{-6}$ a.u. Subsequent coupled cluster with single, double and perturbative triple excitations using the F12 ansatz (CCSD(T)-F12)) calculations and the appropriate auxiliary basis sets yielded accurate determinations of the energies of these three recombination products relative to the ground state *p*-MePhSH molecule. EOM-CCSD calculations were performed to deduce the first few electronic excitations and associated oscillator strengths of each isomer. PECs in the S–H stretch dimension for *p*-MePhSH are reproduced from our earlier study [17] alongside the calculated $S_n \leftarrow S_1$ transition dipole moment (TDM) for each transition that make up the S_1 excited state absorption (ESA) spectrum [17] and $S_n \leftarrow S_0$ TDMs.[15] Equivalent PECs for the first

three triplets states were calculated using an identical methodology to that used in ref. 17 (CASPT2(10/9)/aug(S)-cc-pVTZ). All *ab initio* calculations were performed in Molpro. [30]

III. Results

(i) UV absorption spectra

Static room temperature UV absorption spectra of *p*-MePhSH in the vapor phase, cyclohexane and ethanol solution are displayed in Fig. 1(a). Fig. 1(b) shows an expanded version of Fig. 1(a) between 250 – 310 nm focusing on the wavelength region of current interest. The vapor phase spectrum rises gently at $\lambda < 300$ nm, showing some diffuse vibrational structure at long wavelengths; this band is attributed to $S_1 \leftarrow S_0$ excitation.[15] The absorption cross-section rises more steeply at λ ~265 nm and again at λ ~245 nm. Guided by the results of electronic structure calculations (presented in Fig. 1(c)) and from the dynamics observed in HRA-PTS studies of the same molecule in the gas phase, it is reasonable to associate these latter stronger absorptions with the $S_2 \leftarrow S_0$ and $S_3 \leftarrow S_0$ excitations, respectively.[15] The $S_1 \leftarrow S_0$ feature in the UV absorption spectra of *p*-MePhSH in ethanol and cyclohexane solution appears to be red-shifted by ~2-3 nm relative to the vapor phase spectrum. Remnants of the vibrational structure associated with the $S_1 \leftarrow S_0$ transition are evident in ethanol and, as expected, more clearly in cyclohexane (see Fig. 1(b)). The shoulder observed in the gas phase absorption spectrum of *p*-MePhSH at ~255 nm is still clearly present in cyclohexane, but is no longer discernible in the spectrum in ethanol. Relative to the gas phase spectrum, the peak of the $S_3 \leftarrow S_0$ absorption band at ~240 nm is red-shifted (by ~7 nm) in both ethanol and cyclohexane, and the red wing of this feature is clearly broadened in ethanol.

(ii) Transient absorption spectroscopy

TA experiments were performed in ethanol at four UV excitation wavelengths between 295 – 267 nm; the various pump pulses used are represented with Gaussians under Fig. 1(b). Comparison with *ab initio* theory and gas phase photofragmentation studies [15] suggests that these pump wavelengths will excite the S_1, S_2 and perhaps the S_3 excited electronic states [31] of *p*-MePhSH. As the pump wavelength is tuned across this wavelength region, we expect that different excited states will be initially populated and lead to a notable wavelength dependence in the ensuing dissociation dynamics. First, we investigate the early time dynamics of *p*-

MePhSH with a 270 nm pump pulse which, with the shortest pump pulse width (40 fs), attains the highest time resolution. Fig. 2(a) displays TA spectra acquired at a selection of pump−probe time delays between 0 and 200 fs. At t = 0 fs, there is a peak centered at ~363 nm, which rapidly decays with increasing pump-probe time delay. At t = 200 fs, the intensity is greatly reduced, consistent with our previous photodissociation studies of *p*-MePhSH in ethanol [16] and cyclohexane,[17] which showed the same peak with a very small intensity at t = 200 fs. Fig. 2(b) displays respective data for λ_{pump} = 295 nm, where the 363 nm feature is again present. In both datasets, the center wavelength of this feature coincides well with the calculated $\tilde{D} \leftarrow \tilde{A}$ transition of the *p*-MePhS radical (red bars shown in Fig. 2) as we had tentatively assigned before.[16,17] In general, TA data at t = 0 fs have coherent signals that arise from the temporally overlapped pump and probe pulses, for example, the transient spectrum may contain a coherent contribution from two photon absorption (2PA) of the solvent [32,33] and solute. We will return to discuss this problem and to definitively identify this 363 nm feature in section IV and, in the interim, provisionally assign this feature to *p*-MePhS($\tilde{A}$) radical absorption.

In Figs. 2(a-b) at t = 0 fs, the spectra contain two other features; a band between 425–550 nm associated with the *p*-MePhS($\tilde{X}$) radical ($\tilde{C} \leftarrow \tilde{X}$ and $\tilde{B} \leftarrow \tilde{X}$ absorption bands, violet bars);[15-17,34-36] and an underlying absorption that spans the whole λ_{probe} region, which we have previously assigned to S_n–S_1 ESA using our prior EOM-CCSD/aug-cc-pVTZ calculations (green bars).[17] Focusing on the higher time resolution data for 270 nm photolysis, within the first 200 fs, the underlying absorption decays and the ratio of the *p*-MePhS($\tilde{A}$) (363 nm) and *p*-MePhS($\tilde{X}$) (425 – 550 nm) radical signals inverts. A spectral target analysis [37] that globally fits the time evolving spectrum shown in Fig. 2(a) during the $0 \leq t \leq 300$ fs period allows us to extract three spectral components associated with these simple early time kinetics, including the shape of the S_n–S_1 ESA broad absorption (see the Electronic Supplemental Information (ESI) for details of the target analysis). The three spectral forms present as early time species and their relative populations are shown in Figs. 2(c) and 2(d), respectively. We denote the initially excited state as "S^*" recognizing that 270 nm excites an admixture of different electronic states. We note that the shape of the S_n–S_1 ESA at long probe wavelengths resembles that found in TA for the related *p*-MePhSMe system where the S_1 state is much longer lived.[25,26]

Fig. 3 shows equivalent data for *p*-MePhSH pumped at 267 nm but concentrates on longer time dynamics, 200 fs $\leq t \leq$ 50 ps. The TA are now dominated by absorptions arising from *p*-MePhS($\tilde{X}$) radicals. These bands appear to narrow with increasing pump-probe time delay as the nascent vibrational excitation thermalizes through solute-solvent interactions and, as Fig. 3(b) shows, persist with significant absorption out to long delays (200ps). When considering the fact that the underlying absorption clearly drops away during the first ~5ps, as seen most readily by following the red end of the probe window in Fig. 3(a), it is evident that the $\tilde{X}$ radical population must in fact be rising during the period from 200 fs to 5 ps. A new feature at λ_{probe} ~385 nm develops on much longer (t > 5 ps) time scales that we have previously assigned to adduct formation.[16,17] The formation mechanism of this adduct is considered in section III(iv).

Figs. 4(a) and 5(a) present the corresponding TA spectra measured at the same five pump-probe time delays, for λ_{pump} = 285 and 295 nm, respectively. Consistent with data acquired at shorter excitation wavelengths, these TA spectra show formation of *p*-MePhS($\tilde{X}$) radicals within the longer instrument response time (~150 fs) for these pump pulses. The band we have provisionally associated with *p*-MePhS($\tilde{A}$) radicals is present at the earliest time delays, but is prominent for longer. For example, compare the t = 200 fs data for the 285 and 295 nm pump pulses with that seen at 267 nm. Figs. 4(b) and 5(b) show that the *p*-MePhS($\tilde{A}$) band and much of S_1 ESA signal at λ_{probe} ~600 nm decline rapidly. The S_1 ESA has a greater relative amplitude and clearly rises more towards long probe wavelengths at early delays for λ_{pump} = 285 nm (Fig. 4(a)) than in the 267 and 295 nm data, (see Figs. 3(a) and 5(a), respectively).

Fig. 6(a) compares the pump-probe anisotropy spectra at 200 fs for λ_{pump} = 267, 285 and 295 nm, calculated using eqn. (1). For TA data acquired at 267 and 270 nm (the latter is not shown), the early time anisotropy is positive across the entire probe wavelength range, with the value of $R(t$ = 200 fs) being noticeably more positive across the probe wavelengths associated with ground and excited state *p*-MePhS radicals. Anisotropy spectra recorded at λ_{pump} = 285 nm return $R(t$ = 200 fs) > +0.04 at all probe wavelengths. The respective data at λ_{pump} = 295 nm indicate that the product and excited state absorption signals are negative ($R(t$ = 200 fs) ~ –0.08) across the probe wavelength range, again with the anisotropy being slightly more negative at

probe wavelengths where the *p*-MePhS $\tilde{X}$ and $\tilde{A}$ radicals absorb. Fig. 6(b) shows the anisotropy decay, $R(t)$, for the *p*-MePhS($\tilde{X}$) radical band centered at 500 nm. For the 267 nm pump pulse a clear, ~8 ps, depolarization timescale is determined by fitting; for the other pump wavelengths it is harder to discern the anisotropy evolution, if any, due to a small initial value (285 nm) or poor signal-to-noise (295 nm). Wavelength resolved anisotropy spectra at larger values of pump-probe time-delay (10 ps, data not shown), reveal that the region where the adduct transient rises (385 nm) is mostly depolarized and thus $R(t = 10\ \text{ps}) \sim 0$.

Since the sign of anisotropy is of essential importance to characterizing the initially excited state, here we wish to establish the uncertainty and reproducibility of the measurements shown in Fig. 6. A conservative estimate of the noise level for our TA apparatus is 0.1 mOD, from which we can calculate that the standard deviation for the anisotropy spectra obtained at 295, 285 and 267 nm pump (Fig. 6(a)) is 50%, 10% and 15%, respectively. The larger uncertainty at 295 nm pump is due to the lower signal level. However, we stress that the sign of the initial anisotropies (at 200 fs) for 295 nm and 285 nm pump, albeit small, are reproducible with two different measurement methods – both sequential measurements of TA spectra and simultaneous measurements of kinetics at 500 nm gave consistent results (See ESI for detail).

(iii) Fluorescence Measurements

In our earlier work, we originally assigned the hundreds of picoseconds component of the broad featureless excited state absorption to S_1 ESA.[16] This same offset can be seen in the 600 nm probe kinetics for all pump wavelengths in the current study right out to the longest delays recorded (Figs. 3(b), 4(b) and 5(b)). Our prior assignment was based on fluorescence results from Riyad *et al.* who reported fluorescence at 310 nm with quantum yield = 0.002, and characterized by bi-exponential decay (1.35 and 0.05 ns) for *p*-MePhSH in ethanol. [38] Using the gas phase dynamics [15] as a starting point to explain our observations, it is difficult to reconcile direct dissociation on S_2, or ultrafast tunneling from the S_1 state, that is indicated from the instantaneous *p*-MePhS radical formation evident in Figs. 2-5, with even a small population held up in S_1,[38] and an associated nanosecond lifetime. We therefore sought to reproduce and verify the literature fluorescence measurements for *p*-MePhSH in different solvents.

Our attempts to measure a fluorescence spectrum and lifetime for *p*-MePhSH revealed two key issues: (*i*) in cyclohexane, there is virtually no fluorescence if the solution is properly flowed ($\Phi_F < 10^{-5}$). (*ii*) Without flowing the solution, the emission spectrum in both alcohols and cyclohexane is extremely sensitive to photodegradation even under illumination in a Xenon lamp fluorimeter for minute-long exposures. These experiments are detailed in the ESI. In short, we find that irradiated solutions rapidly produce a new fluorophore which must arise from a photochemical product. The similarity between the fluorescence spectra of the photoproduct induced by illumination and those reported for thiophenol by Riyad *et al.* casts some doubt on the reliability of their steady-state fluorescence spectra and thus any long-lived S_1 population.

Fortunately, we find that the UV/visible absorption spectrum also tracks the photoproduct build up from the UV photochemistry that is seen more emphatically in the fluorescence spectrum. We can use this to monitor any such photochemical build up in the ultrafast TA experiments which use a wire-guided gravity jet: None are apparent after 45 minutes of laser exposure. Details of this procedure and such evidence are also presented in the ESI.

(iv) Recombination to form adduct: calculations of structure and spectra

In our previous studies of *p*-MePhSH,[16,17] we asserted that the TA signal centered at 385 nm which rose at $t > 5$ ps and on a timescale coincident with the decay of the *p*-MePhS($\tilde{X}$) band originated from recombination of *p*-MePhS and H geminate partners to form an adduct, instead of reforming the dissociated S–H bond. The timescale in which this signal rises and the *p*-MePhS($\tilde{X}$) radicals are depleted is in good agreement with recent UV pump, mid-IR probe measurements assigned to radical decay and ground state recovery in acetonitrile and cyclohexane.[25,26] We can further rationalize the assignment to a *p*-MePh(H)S adduct on several grounds: the rise time of the adduct feature is insensitive to *p*-MePhSH concentrations (45 and 90 mM), which allows us to rule out a bimolecular reaction between either *p*-MePhS or H atoms and ground state *p*-MePhSH or excimer formation – the latter we recently observed in PhOH.[17]

The 385 nm TA band has a similar peak wavelength and band shape to that observed in the pulsed radiolysis PhSH data from Riyad *et al.*[38] These authors however assigned the band to an open-shell PhSH(H) product– *i.e.* where an H atom forms a bond with a ground state molecule, The time resolution of the flash-photolysis apparatus used by Riyad *et al.* is limited to ~ 1 μs,[38]

but we have the significant advantage of being able to probe the early time dynamics and see the simultaneous decay of the *p*-MePhS($\tilde{X}$) radical with the rise of this new transient.

Here, we observe the same adduct formation at all photolysis wavelengths used; we note that this applies also to 200 nm excitation previously reported.[16,17] We now seek to clarify the identity of this TA with high-level *ab initio* CCSD(T)-F12//MP2/aug-cc-pVTZ ground and EOM-CCSD/aug-cc-pVTZ excited state calculations. The results are summarized in Fig. 7, where all energies for *p*-MePh(H)S isomers are given relative to the S_0 minimum of *p*-MePhSH.[15] The S_0 minima for each of the three isomers lie below the *p*-MePhS + H radical asymptote (3.48 eV). Assuming that the energies of the transition states also lie below this asymptote, we can conclude that all three are plausible products of a recombination reaction between the two radicals. The ground states of isomers A, B and C lie, respectively, 0.96, 2.56 and 1.02 eV above the minimum energy of *p*-MePhSH. The energies of the excited electronic states vary, however, as do the respective oscillator strengths. Each isomer of the adduct has only one transition with large oscillator strength at energies below 6.5 eV (see Fig. 7). The vertical excitation energies to the 'bright' states of isomers A (the S_2–S_0 transition) and B (S_4–S_0 transition) match better with the ~385 nm band observed in the present spectra; the lowest energy transition of isomer C with appreciable oscillator strength is calculated to lie at significantly shorter excitation wavelengths (~270 nm) and outside of the present probe wavelength range.

IV Discussion

The gas phase photodissociation dynamics of *p*-MePhSH provide a rich set of observables revealing a reaction energy disposal that varies with excitation wavelength,[15] including the recoil, the nascent vibrational excitation and the $\tilde{X}/\tilde{A}$ branching in the *p*-MePhS products. In solution, both alternative channels and new layers of dynamical complexity are present even for bond dissociation, such as solvent influence on passage through each CI, caging, electronic quenching by return passage through the S_2/S_0 CI, and vibrational cooling. First, our studies show no evidence for photoionization, an alternate channel available for aromatics excited above the likely threshold for adiabatic ionization in polar solvents.[39] Photoionization of *p*-MePhSH is ruled out from our results as no transients associated with *p*-MePhSH$^{\bullet+}$ cations, which have been

characterized to absorb at 550 nm in *n*-butyl-chloride,[36] or solvated electrons [40,41] are present in any of our TA data, even with 200 nm excitation[16] Second, clear observation of one product of the photodissociation process, the *p*-MePhS($\tilde{X}$) radical, is observed within our instrument response time irrespective of the initially excited state from 295 to 200 nm.[16,17] However, evidence for the *p*-MePhS($\tilde{A}$) formation was only tentative in our previous studies[16,17] because of the ultrafast electronic quenching of this transient. Here, by carefully considering the earliest time delay TA data, we are able to confirm observation of the MePhS($\tilde{A}$) radical and deduce the nascent $\tilde{X}/\tilde{A}$ branching ratios as a function of excitation wavelength in the solution phase.

Our TA data also show spectral narrowing of the *p*-MePhS($\tilde{X}$) radical product over longer time delays, as the initially hot radicals dissipate their energy into the solvent bath on a picosecond timescale. Although differing widths in the nascent *p*-MePhS($\tilde{X}$) electronic absorption can be observed, most notably in our previous study employing 200 nm excitation,[16,17] this vibrational cooling is more easily quantified in UV-IR pump-probe data as there are far fewer overlapping features in the mid-infrared probe region.[25,26] On the other hand, information on the initial translational energy release at the different excitation energies is readily recovered by analysis of the longer-delay diffusive geminate recombination. We will quantify the initial separation of the geminate partners and show that it depends strongly on the excess energy provided by the pump photon.[16,17,42,43] This approach allows us to explore the H atom translational energy release in solution as a function of excitation wavelength and solvent, which we can then directly compare back to the gas phase photofragmentation dynamics.

(i) Wavelength dependent excitation and dissociation mechanism

Gas phase experiments have demonstrated that the $\tilde{X}/\tilde{A}$ radical product branching is determined at the S_2/S_0 CI,[15,20-22] but that the equilibrium geometries of the initial and the photoexcited states are also crucial in determining the final radical product branching ratio.[15] This can be understood by recognizing that the planarity (or otherwise) of the S–H bond and the aromatic ring controls whether flux approaching the S_2/S_0 CI follows the diabatic path to *p*-MePhS($\tilde{X}$) radicals or the adiabatic surface yielding *p*-MePhS($\tilde{A}$) products. The preferred geometry at this CI is controlled by the forms of the S_0, S_1 and S_2 torsional potentials in the vertical Franck Condon (vFC)

region.[15] For *p*-MePhSH, theory predicts that the ground and S_1–S_3 excited states all have planar geometries – thereby accounting for the observed preference for *p*-MePhS($\tilde{X}$) radical formation at all excitation wavelengths investigated in the gas phase.[15]

In a polar, strongly interacting solvent such as ethanol, however, the relative position and topologies of PES can be shifted and it is not possible to assume that for a given excitation wavelength the state excited in the gas phase is necessarily the same in solution. This is evident from the static UV absorption spectra: the shoulder at ~255 nm, observed in both gas phase and cyclohexane solution, is either greatly diminished or perhaps shifted in ethanol solution (see Fig. 1(a)), hinting that the polar solvent has a differential effect on the oscillator strength and/or center wavelength of the $S_2 \leftarrow S_0$ transition. Given the typically large permanent dipole moment of $^1\pi\sigma^*$ states and that the $\sigma^* \leftarrow \pi$ electron promotion is "charge-transfer" in nature,[1] it seems reasonable that a polar solvent affects this particular state more dramatically than $^1\pi\pi^*$ states.

To expand on this last point, calculations on the isolated molecule show that the $\sigma^* \leftarrow \pi$ transition dipole moment (TDM) in the vFC region is stronger than for the corresponding transition in phenol,[15,24] reflecting the reduced Rydberg character and thus greater orbital overlap. This also explains the smaller permanent dipole moment of the $^1\pi\sigma^*$ state of *p*-MePhSH (*cf.* phenol), as the largely valence σ^* orbital is more localized on the S–H bond (*cf.* the greater O(3*s*) Rydberg contribution in the corresponding orbital in phenol); the former state thus has less charge-transfer (CT) character. Given the differences in the permanent dipole of the S_2 state relative to those of the S_0, S_1 and S_3 states, solvation with a polar solvent would be expected to cause a relative destabilization of the $^1\pi\sigma^*$ state and an increase in the S_2–S_1 energy gap in the vFC region (*cf.* gas phase).

The analysis of the surface shifts is, however, a little more involved: we need to also consider how Rydberg/valence mixing, and thus CT character, might be influenced by the solvent environment. The O(3*s*)/S(4*s*) component constitutes the first member of a Rydberg series that converges to the first ionization potential, which, in the case of *p*-MePhSH in ethanol, is ~1.1 eV lower than the gas phase value.[44,45] We can also anticipate that an extended Rydberg orbital will experience increased (destabilizing) Pauli repulsion in the close-packed solvent

environment. If the net effect of these two contributions is stabilizing, then we should expect greater $^1\pi 4s/^1\pi\sigma^*$ mixing in ethanol than in the isolated molecule, a reduction in $S_2 \leftarrow S_0$ TDM and greater destabilization of the S_2 state. But it could also change the topology of the S_2 PES in the S–H stretch coordinate, lowering the energy in the vFC region where the Rydberg mixing is highest, [46] thereby introducing a "shelf" in the S_2 potential that would mitigate some of the expected solvation-induced blue shift.[47] In this scenario, it is unclear whether the barrier under the S_1/S_2 CI would increase or decrease and thus how the tunneling rate and S_1 lifetime might change relative to that of the isolated molecule. Conversely, if the net effect of ethanol solvation is to destabilize the Rydberg component, the differences between the gas and solution phase environments would be less. In this scenario, the S_2 state would have even greater $^1\pi\sigma^*$ character than in the isolated molecule, the S_2 PES would be purely repulsive, the permanent dipole moment of the S_2 state would be reduced and the $S_2 \leftarrow S_0$ TDM would be similar, or greater, than in the gas phase. The assumed reduction in Rydberg character and any residual solvent-induced destabilisation would tend to increase the vertical S_2–S_0 gap, leading to a blue-shifted absorption in ethanol, and to reduce the tunnelling rate from the S_1 state. The latter scenario seems more consistent with the changes in absorption spectrum (Fig. 1), though we concede that the reduced $S_2 \leftarrow S_0$ oscillator strength implied by the first scenario could also be consistent with Fig. 1.

Pump-probe anisotropy provides a means to correlate the relative orientation of the initially excited molecule with the resultant radical TDMs and thus elucidate the initially populated excited state(s). In the limit that the TDMs of the pumped and probed species are rigorously parallel or perpendicular to one another, $R(t \rightarrow 0$ fs) takes the limiting values of +0.4 and –0.2, respectively. Electronic structure calculations[16] have shown that the *p*-MePhS($\tilde{X}$) radical absorption in the range 425–550 nm encompasses the (strong) $\tilde{B} \leftarrow \tilde{X}$ and (weaker) $\tilde{C} \leftarrow \tilde{X}$ transitions and that the $\tilde{D} \leftarrow \tilde{A}$ and $\tilde{B} \leftarrow \tilde{X}$ TDMs are parallel to the C–S bond.[16] The parent S_1–S_0 and S_2–S_0 TDMs are both calculated to lie perpendicular to the C–S bond, while that for the S_3–S_0 transition is aligned along the C–S bond.[15-17] The anisotropy measurements show $R(t$ = 200 fs) is relatively flat across the probe wavelengths for a given excitation wavelength and evolves from slightly negative (~ –0.05) to positive (~ +0.15) as λ_{pump} is reduced from 295 nm to

267 nm, with the spectra exhibiting somewhat greater anisotropy where the $\tilde{X}$ and $\tilde{A}$ state radicals absorb (see Fig. 6).

From our assignments of spectral features in the TA spectra, we can start to disentangle what determines $R(t \rightarrow 0$ fs). Let us first concentrate on the 425–550 nm band associated with *p*-MePhS($\tilde{X}$) absorptions. This absorption is dominated by the $\tilde{B} \leftarrow \tilde{X}$ radical TDM that lies parallel to the C–S bond (see Fig. 1(f)), with a minor contribution from the $\tilde{C} \leftarrow \tilde{X}$ transition at shorter wavelengths that has a TDM which lies at an angle of ~68° to the C–S bond, but rides on a structured part of the S_1 ESA spectrum (see calculated ESA spectrum in Figs. 2 and 3).[17] The $\tilde{X}$ and $\tilde{A}$ states have a splitting of 3320 cm^{-1} (ref. 15) and may well undergo vibronic mixing and these electronic structure calculations do not account for these effects. This will therefore directly impact upon the direction and the order of magnitude of the calculated radical electronic TDMs [16] and might also account for the non-limiting observed values of $R(t)$ as noted above. For the remainder of this part of the discussion, we shall concentrate on the strong $\tilde{B} \leftarrow \tilde{X}$ radical transition, which lies parallel to the $\tilde{D} \leftarrow \tilde{A}$ radical transition. From the three possible parent TDMs, only the S_3–S_0 TDM lies parallel to the $\tilde{B} \leftarrow \tilde{X}$ radical TDM, and thus at 267 and 270 nm we ascribe the parent absorption in this region mainly to $S_3 \leftarrow S_0$ excitation. This is in contrast to that inferred from the gas phase photofragmentation studies[15] but is consistent with the observed bathochromic shift in the linear absorption spectrum (see Fig. 1(a)). It is clear from our TA spectra, however, that the S_3 state must undergo rapid coupling to the dissociative S_2 so as to produce *p*-MePhS radicals within our instrument response time.

For the longest pump wavelength studies, a negative $R(t)$ is observed, which is consistent with either the $S_2 \leftarrow S_0$ or $S_1 \leftarrow S_0$ parent transitions, as both lie perpendicular to the $\tilde{B} \leftarrow \tilde{X}$ radical TDM. Given the similarity of the absorption spectrum at this wavelength to that of the vapor phase sample and the predictions from electronic structure calculations, we favor the interpretation involving $S_1 \leftarrow S_0$ excitation and subsequent rapid tunneling under the S_2/S_1 CI to the dissociative S_2 state (*i.e.*, the same mechanism as that invoked to explain the gas phase behaviour [15]). The value of $R(t = 200$ fs) obtained at 285 nm is less obvious to interpret. Given the potentially shifted $\sigma^* \leftarrow \pi$ transition in the ethanol absorption spectrum (and the lack of data

in cyclohexane at this pump wavelength), we are presented with several possibilities which require invoking the initial population of two excited states as the value of $R(t)$ returned is not close to the limiting values. Only an initial admixture of S_1 and S_3 or S_2 and S_3 states can reconcile this observation, but this requires that the S_3–S_0 parent absorption stretch to far longer wavelengths in ethanol than discerned in gas phase experiments. Although consistent with the shift in the S_3–S_0 absorption band peak upon solvation (see Fig. 1(a)),[15,16] we find this conclusion somewhat surprising.

(ii) *p*-MePhS $\tilde{X}$ / $\tilde{A}$ product branching

Armed with an understanding of the clear differences in PESs of *p*-MePhSH between the solution and gas phases, at least in the vFC region, we now turn our attention to the electronic branching of *p*-MePhS radicals. The TA spectra acquired between 0 – 200 fs at 270 nm where the pump pulse duration is shortest, reveal a feature at 363 nm within the ~50 fs instrument response time, see Fig. 2(a). This feature survives beyond the time window where pump and probe pulses overlap, but decays rapidly. We obviously wish to track the evolution of this feature from t = 0 fs onwards and thus need to understand the spectral evolution of this feature during the temporal pulse overlap. Conventional wisdom would suggest that signals within pump-probe overlap contain a large coherent pump + probe component to the signal, for example from 2PA of the solvent or resonant 2PA or Raman from the solute, which can contaminate the transients arising from the evolution of the excited state molecules. It is important to recognize that when the two pulses are overlapped, if this peak were to arise from a coherent interaction such as two-color 2PA, it would shift as a function of pump excitation energy. Fig. 2 displays data acquired at 270 and 295 nm, and it is apparent that the feature does not shift in probe wavelength. The expected shift for a signal originating from 2PA when pumping at 295 vs. 270 nm would be ~40 nm (see details in ESI). This observation allows us to rule out any contribution in the 363 nm transient from 2PA. The center wavelength of this transient corroborates well with the calculated *p*-MePhS($\tilde{D} \leftarrow \tilde{A}$) transition (red bars in Figs. 2 and 3), and the decay of this feature is commensurate with the rise of the *p*-MePhS($\tilde{X}$) radical absorption band. We are therefore confident to assign this feature to nascent *p*-MePhS($\tilde{A}$) radicals, in line with the expectation from gas phase experiments that excited state radicals are formed. Murdock *et al.* did not observe the vibrational signatures of *p*-MePhS($\tilde{A}$) radical

products when photodissociating *p*-MePhSH in acetonitrile or cyclohexane, but these authors utilized a flow cell with CaF_2 windows to deliver the sample solution which reduced the experimental response time to ~1 ps.[25] Considering that we can only just glimpse the electronic signature of *p*-MePhS($\tilde{A}$) radicals at t = 200 fs, it is not surprising that this extremely short-lived species was not observed given the lower time resolution of the IR probe experiment.

Now that we have confirmed the generation of both *p*-MePhS($\tilde{X}$) and ($\tilde{A}$) radicals, can we extract the initial electronic branching ratio in ethanol solution? Fig. 2 shows that the band area attributed to the *p*-MePhS($\tilde{A}$) radical in TA spectra acquired at λ_{pump} = 270 and 295 nm and t = 0 fs is far greater than that of the *p*-MePhS($\tilde{X}$) radical, but to derive their relative populations we would normally require the respective extinction coefficients. *Ab initio* calculations predict that the absorption cross section of *p*-MePhS($\tilde{A}$) radical is very much smaller than that of the *p*-MePhS($\tilde{X}$) radical (see Fig. 2 violet and red bars), however, we can clearly observe the $\tilde{A}$ state radicals in solution and this brings into question the reliability of the magnitude returned by the calculated TDMs. As noted earlier, we recognize that these particular calculations are likely to be susceptible to problems involving vibronic mixing of the two close-lying states.

We can avoid the need for extinction coefficients of the radical species, however, by considering the initial yield of the *p*-MePhS($\tilde{X}$) state radical and its rise in the first few hundred femtoseconds, and what precursor species might feed its production. The fact that the *p*-MePhS($\tilde{X}$) band rises as the $\tilde{A}$ state falls when excited at 270 nm (see Fig. 2) is suggestive that $\tilde{A}$ state quenching by re-crossing the S_2/S_0 CI due to caging[11] is one mechanism that produces *p*-MePhS($\tilde{X}$) over this period. This reasoning is confirmed by the target analysis that yields Fig. 2(c,d). This gives us a route to estimate the initial population of *p*-MePhS($\tilde{A}$). For simplicity of explanation, let us for the moment assume that the decay of trapped S_1 (as mapped by the ESA decay) is slower and provides additional *p*-MePhS only later. Comparing the $\tilde{X}$ state radical signals at t = 0 fs and t = 200 fs, after considering the underlying signal due to S_1 ESA, then yields a first estimate on the initial $\tilde{A}$ and $\tilde{X}$ state yields on the basis that all of the $\tilde{X}$ state rise comes from quenching of $\tilde{A}$ state. This in turn provides a lower limit for the initial $\tilde{X}/\tilde{A}$ branching ratio for 270 nm photolysis of 0.15.

While showing why extinction coefficients for each band are not needed *a priori*, the above simplistic analysis neglects the fact that several other processes are taking place in parallel with *p*-MePhS($\tilde{A}$) quenching. Referring to Fig. 1, these include the decay to produce *p*-MePhS($\tilde{X}$) of any initially excited state population held up on S_1 and the possible cage recombination of *p*-MePhS($\tilde{A}$) + H fragments instead of quenching. Inspection of Fig. 1(c) leads us to conclude that upon shortening of the S–H bond some fragments will follow the diabatic path back to reform ground state *p*-MePhSH. Inclusion of these latter processes will tend to decrease our estimate of the initial $\tilde{A}$ state population and thus increase the $\tilde{X}/\tilde{A}$ population ratio compared to our first crude estimate. The target kinetic model used in the spectral fitting (Fig. 2(d)) includes these additional pathways (see ESI which also discusses robustness of fit). We can therefore refine the value for the initial radical populations formed within the 270 nm pump pulse width by inspection of Fig. 2(d) that shows the fitted populations that emerge from spectral fitting. What is obvious from Fig. 2(d) is that the S_1 population evolves over the first 300 fs and supplies a significant fraction of the build-up in *p*-MePhS($\tilde{X}$). Simply comparing the populations at the peak of the pump pulse as a definition of t = 0 fs would give a ratio of $\tilde{X}/\tilde{A}$ = 1.3. However, this points to a deeper problem: how best to extract what we really seek to compare to the gas phase, namely the first pass branching *probabilities*, when we have time evolving populations that have necessarily been convoluted with the instrument response function in order to reproduce the transient spectral evolution? To get closer to this initial branching probability, and recognizing that the first crossing of the conical intersection is likely inside the instrument response of our 270 nm data, we should analyze what the kinetic model is telling us about branching before convolution, through the fitted rate parameters (see ESI for details). This approach yields our best estimate for the $\tilde{X}/\tilde{A}$ first pass branching ratio of 0.8 with 45% of initially excited population not undergoing immediate dissociation (what we have called "trapped" on S_1). Because our model has not included any fresh *p*-MePhS($\tilde{A}$) population emerging from delayed decay of S_1 and the possibility that $\tilde{X}$ population may, like $\tilde{A}$, also be decaying by cage recombination over this period, hidden by the other channels feeding its population, we consider this final estimate of 0.8 as an upper limit for the initial branching ratio.

It is useful to compare to data recorded in cyclohexane at this same pump wavelength (λ_{phot} = 270 nm) reproduced in Fig. 8.[17] Here the radical $\tilde{A}$ band is much more pronounced and blue shifted compared to ethanol. The characteristic shape of the $\tilde{X}$ band is not visible in the t = 0 fs slice. Analysis of the data in Fig. 8 with an identical kinetic model yields an $\tilde{X}/\tilde{A}$ branching ratio of 0.03 (see ESI for populations and decay associated spectra); *i.e.* very few *p*-MePhS($\tilde{X}$) fragments appear to be formed on first pass through the CI in cyclohexane. Although it is clear the uncertainty of these branching estimates depend sensitively to assumptions about processes parallel to the quenching of $\tilde{A}$ to $\tilde{X}$, they do establish that $\tilde{A}$ state radicals are the dominant products at 270 nm, and more so in cyclohexane than in ethanol. In other words, upon dissociation and encounter of the S_2/S_0 CI, most molecules avoid crossing onto the lower adiabat.

Because of the lower time resolution of the 285 and 295 nm data sets, it is more difficult to use target analysis to extract the time-evolution and branching in the same way. However, we can utilize the amplitudes of the *p*-MePhS($\tilde{A}$) and *p*-MePhS($\tilde{X}$) spectral bands extracted from the target analysis (Fig. 2(c)) to get an estimate for the extinction coefficient ratio. The transition associated with $\tilde{A}$ state radicals has ~2.6 times the peak intensity of that originating from $\tilde{X}$. With this information in hand, we can qualitatively extract the immediate yields of the two radical channels by inspection of the t = 0 fs slices, taking into consideration the underlying S_1 absorption. This rough analysis yields $\tilde{X}/\tilde{A}$ ratios of ~0.5 at 270 nm, and ~1.0 at 285 and at 295 nm. Although relatively greater branching to $\tilde{X}$ state products is observed at these longer wavelengths, we note that the $\tilde{A}$ state yield is prominent for at least 200 fs in Figs. 4 and 5, which could mean that the rate of *p*-MePhS($\tilde{A}$) quenching, or the rate of predissociation (*i.e.* tunneling out of the S_1 state to S_2), slows on decreasing the excitation energy.

The deduced solution phase initial branching ratios differ with those observed in the gas phase, where at all wavelengths branching at the S_2/S_0 CI is characterized by yields favoring $\tilde{X}$ over $\tilde{A}$ state *p*-MePhS radicals with this propensity increasing at shorter photolysis wavelengths. Specifically, the $\tilde{X}/\tilde{A}$ branching ratio was found between 1.1 and 1.5 in the range $293.5 \geq \lambda_{pump} \geq 286.2$ nm and ~1.7 at $\lambda_{phot} < 240$ nm.[15,48] The gas phase study of several *para*-substituted thiophenols showed that the $\tilde{X}/\tilde{A}$ branching fraction was determined by the degree of excitation

in out-of-plane S–H torsional motions, or non-planarity at the S_2/S_0 CI.[15,20-22] These studies were performed in a jet-cooled molecular beam, however, whereas the TA experiments in cyclohexane and ethanol were performed at T = 298 K (where k_BT = 207 cm^{-1}). The depth of the S_0 potential, which has a minimum at planar geometries, was found to be 145 cm^{-1} (at the CCSD(T)-F12/aug-cc-pVTZ level).[15] It is clear that even isolated *p*-MePhSH molecules at 298 K would be less biased in favor of planarity – thus reducing the preference for following the diabat to $\tilde{X}$ state products. More significantly, for a solution environment, diffusional motion rather than free motion will be executed in the torsion coordinate. Therefore, solvent molecules proximal to the *p*-MePhSH will act to "lock" the conformational distribution on photoexcitation. This in turn will serve to impede any motion that drives the molecule in vacuum towards planarity prior to reaching the S_2/S_0 CI. This realization perhaps explains why the $\tilde{X}/\tilde{A}$ branching ratio is so low in cyclohexane. The less extreme branching in ethanol (*cf.* cyclohexane) can be explained as ethanol may act as a weak hydrogen bond donor to the sulfur atom,[49] and this may enhance the bias on the free energy surface toward planarity compared to a non-hydrogen-bonding solvent like cyclohexane. Any effect that increases the equilibrium population within a cone around planarity will increase the $\tilde{X}$ state yield.

(iii) Diffusive Geminate Recombination

The cage recombination discussed above, in which the *p*-MePhS radical and the H atom encounter the first solvent shell and recombine within our instrument response time, leads to an unsuccessful dissociation event. A successful dissociation, on the other hand, creates a distribution of escape distances separating the H + *p*-MePhS($\tilde{X}$) products, as dictated by the excess energy provided by the photon above the energy required to break the S–H bond.

The average separation distance, or the ejection length, of the H atom formed in ethanol can be further quantified in a similar way to that employed in our previous study,[16] wherein we *simultaneously* fitted the decay of the *p*-MePhS($\tilde{X}$) radical signal and the rise of the adduct signal in a model that included radical-radical geminate recombination.[27] It is important to stress that we consider the *entire* band of the *p*-MePhS($\tilde{X}$) radical (425 – 550 nm) and that of the adduct (350 – 400 nm), by using Gaussian functions but with amplitudes that are allowed to fit as a function of *t*. We used a similar approach to account for the underlying long-lived ESA

signals. In the geminate recombination model, a geminate pair of radicals is created instantaneously at a separation distance (r_0) followed by diffusion through solvent, and when they encounter each other within the reaction radius (r_{xn}), recombination is assumed to be instantaneous as it proceeds without a barrier.[27] Thus, the survival probability and thus the normalized TA signal can be described by the following equation:[50]

$$\mathrm{TA}(t) = \mathrm{erfc}\left(\frac{r_{xn}}{\sqrt{4D't_g}}\right) + \frac{r_{xn}\exp\left[-r_{xn}^{\,2}/4D'\left(t+t_g\right)\right]}{\sqrt{\pi D'\left(t+t_g\right)}}\left[\mathrm{erfc}\left(\sqrt{\frac{r_{xn}^{\,2}t}{4D't_g\left(t+t_g\right)}}\right)\right], \qquad (2)$$

where *erfc* is the complementary error function. We estimated the value for r_{xn} to be 2.7 Å, similar to that for H + OH recombination in H_2O.[51] D' is the sum of the diffusion coefficients, D_H and $D_{p\text{-MePhS}}$, in ethanol solution. We assume that $D_{p\text{-MePhS}}$ is close to $D_{benzene}$ in ethanol = 1.88 x 10^{-4} $Å^2$ fs^{-1} (Ref. 52). For D_H, we use 6.38 x 10^{-4} $Å^2$ fs^{-1}, derived from D_H in water [53] and account for the difference in the viscosities of ethanol and water using the Stokes-Einstein equation. t_g is related to the width of the distribution of H atom ejection lengths, which is assumed to be Gaussian and determined by fitting. The width is related to the average ejection length, $\langle r_0 \rangle$, as the Gaussian is centered at the origin, and thus:

$$\langle r_0 \rangle = (8\pi)^{1/2}\sqrt{2D't_g}\,. \qquad (3)$$

From fitting, these average ejection lengths, $\langle r_0 \rangle$, were found to be 4, 6 and 9 Å for excitation at 295, 285 and 270 nm, respectively, representing a variation of H atom ejection of ~1–3 solvent spheres. Notably, the ejection length of 9 Å at 270 nm is in excellent agreement with that reported previously,[16] where the decay kinetics of the *p*-MePhS($\tilde{X}$) radical were monitored at a single wavelength (500 nm). In cyclohexane, the ejection length fitted for geminate recombination also increased from 9 to 12 Å when the photodissociation wavelength was decreased from 267 nm to 200 nm, with a concomitant increase of 3500 cm^{-1} in the average kinetic energy release determined in the gas phase.[17]

The recombination yield is ethanol is highest at 295 nm and lowest at 267 nm pump excitation. This is also in broad agreement with the gas phase H atom photofragment translational spectroscopy experiments whereby decreasing the photolysis wavelength led to a modest increase in the H atom kinetic energy released over the same range of excitation wavelengths,[15] despite the photon energy increasing by ~3500 cm^{-1}. The majority of the extra photon energy is

in fact partitioned into additional *p*-MePhS product vibrational energy. This has been rationalized by noting that the shorter wavelength excitations within this range favor population of vibrationally excited levels of S_1, and that this vibration maps through into the *p*-MePhS radical upon S–H bond fission. Upon tuning to wavelengths where the S_2 state is directly populated (*e.g.* 266 nm in the gas phase), the isolated molecule dissociation dynamics show a step change with most of the photon energy in excess of the S–H bond dissociation energy released as H atom KE.

The solution phase TA experiments show a similar trend over the same pump wavelength range: a gradual increase in photolysis energy leads to an increased H atom ejection length, *i.e.*, the H atom is propelled further from the *p*-MePhS photofragment, and therefore leads to a reduced probability of re-encounter. Conversely, the early time TA spectra shown in Fig. 2 (t = 0 fs in particular) reveal that 267 nm excitation generates a broader contour for the *p*-MePhS($\tilde{X}$) radical than 295 nm - indicative that the radical is formed vibrationally hotter at 267 nm. This apparent difference can be rationalized by reiterating the differential shifts of PECs in the polar, strongly interacting solvent: the dissociative S_2 state may be shifted to higher energy relative to the gas phase potentials, and/or the S_3 state is accessible at 285 nm – as implied by the anisotropy measurements (see Section IV(i)), which then must undergo very rapid coupling to S_2 as *p*-MePhS radicals are observed within our instrument response time.

The identity of the recombination product still remains to be settled and we now address this issue with new high level *ab initio* calculations. This is complemented by recent UV-IR pump-probe experiments [25,26] that monitored directly the ground state bleach recovery (that in the UV was hampered by overwhelming ESA contributions) and radical adduct formation.

(iv) Adduct structure

Our TA measurements were key to recognizing a new transient that rises at t > 5 ps and arises via a geminate recombination pathway wherein the H atom recombines with the *p*-MePhS ring rather than reforming the S–H bond. Our high level ground state CCSD(T)-F12 and excited state EOM-CCSD calculations support this hypothesis, revealing that all three isomers are energetically accessible from the product radical asymptote, assuming the transition state is

downhill. *Ortho* and *meta*- isomers A and B are predicted to display similar electronic absorption spectra (Fig. 7). The EOM-CCSD calculations do not allow for any relaxation of the excited state geometries. We can anticipate that the calculated excitation energies would be lower if this effect were included – thus matching better the absorption band present in the TA data at λ_{probe} ~385 nm. Adduct C, however, does not have a transition with appreciable TDM in our TA probe window, so it is impossible for us to assess the population of such species from this method. Our $R(t)$ measurements (Fig. 6) show that reorientation of the *p*-MePhS fragment occurs on a ~8 ps timescale, whereas adduct formation rises at $t > 5$ ps. This means that the H atom and *p*-MePhS co-fragment will re-encounter each other when their mutual orientations are largely randomized, and so a starting picture might be that any bias toward stereochemical selectively in forming adducts is mostly eliminated. Further, if adduct formation is a kinetically controlled reaction, with the transition states to forming each adduct all downhill, then the A, B and C adducts would likely be formed in a 2:2:1 ratio since there are two possible *ortho*- and *meta*- positions but only one *para*- site for H atom "attack". Taking into account the steric hindrance by the methyl group, the *para*- position might be expected to be disfavored. If the reaction is instead thermodynamically controlled, isomer B would be disfavored greatly as it has a ground state that lies ~1.5 eV higher in energy than the A or C minima.

It is important to recognize that the calculated electronic TDMs of the adduct transitions of interest are ~10 times larger than those of the *p*-MePhS($\tilde{X}$) radical; this implies that the TA experiments will appear to exaggerate the relative significance of this channel. UV-IR pump-probe experiments are complementary to the TA experiments reported here and can help confirm the proposed adduct structures and cross-check their relative populations. Previous experiments at λ_{pump} = 267 nm in CD_3CN yielded three small peaks at 1425, 1520, and 1625 cm^{-1} within a 1400–1650 cm^{-1} IR probe window that were tentatively attributed to adduct formation.[25,26] We can use the structures calculated here to estimate the normal modes and associated wavenumbers of the three proposed adduct structures (see ESI for full details) and thereby assign these transitions. To test the reliability of our B3LYP/6-311+G* calculated frequencies with anharmonic corrections, we also calculated the normal modes of the *p*-MePhS($\tilde{X}$) radical. The agreement between the calculated and the experimentally measured wavenumber for the strongest radical transition in this spectral region is good: 1568 *vs.* 1575 cm^{-1}. Inspection of the

calculated normal modes and associated IR intensities revealed that adduct structures A and B each have two strong IR transitions in the 1400–1650 cm^{-1} probe window (at 1532 and 1420 cm^{-1}, and at 1538 and 1418 cm^{-1}, respectively), with the ~1535 cm^{-1} transitions having about twice the intensity of those at ~1420 cm^{-1}. The predicted A and B adduct transitions at 1532 and 1538 cm^{-1} agree reasonably with the observed peak at 1520 cm^{-1}, and the weaker IR transitions predicted at ~1420 cm^{-1} with the peak observed at 1425 cm^{-1}. Structure C is predicted to show only one strong IR peak feature in this region (at 1639 cm^{-1}), in good agreement with the observed peak at 1625 cm^{-1}.

From this analysis, we are unable to rule out some formation of isomer B, because of the similar wavenumber of a strong IR transition of both isomers A and B. We disfavor this possibility, however, on two grounds: (i) if A and B isomers were formed with equal populations, it would be expected that the peak at ~1520 cm^{-1} would be wider compared to the peak at 1625 cm^{-1} which is attributed to one isomer; (ii) adduct B is strongly (~1.5 eV) thermodynamically disfavored. From this three pronged approach using two different experiments and theory, we conclude that the H atom attacks the ring at the *ortho* and *para* positions to form isomers A and C. Steric hindrance by the *para*- methyl group apparently has little role in determining the adduct populations. The relatively fast (~ 5 ps) appearance time for adducts suggests that their formation is barrierless after diffusive re-encounter. The UV–IR work indicates that the predominant recombination reaction is to reform the parent. Indeed, the calculated TDM for electronic probing confirms this observation, suggesting that in ethanol only a few per cent of the recombination products are adduct (see Figs. 3 and 7).

V Conclusions

This paper caps a series of reports from our two groups that compare the detailed photodissociation dynamics of *p*-MePhSH in the gas and solution phase.[15-17,25,26] By exploring the excitation wavelength dependence of the S–H bond scission reaction, we are able to reveal changes in the energy release (vibration, translation, electronic) in the immediate moments of bond breaking and first passage through the S_2/S_0 CI. It is found that irrespective of the initial singlet state excited, $\pi\sigma^*$ state reactivity dominates the early time photochemistry, and despite the spin-orbit coupling from the sulfur atom, no definitive spectral evidence for ultrafast ISC is observed in our TA experiments. Importantly, our electronic TA experiments carried out in a

thin flowing jet have sufficient time resolution to capture the $\tilde{A}$ state *p*-MePhS radical before its electronic quenching within 200 fs. We find that in ethanol at 270 nm, $\tilde{A}$ state radicals dominate after first pass through the S_2/S_0 CI, in contrast to the gas phase result, which favors the *p*-MePhS($\tilde{X}$) radical. In cyclohexane, the inversion in favor of $\tilde{A}$ state radicals is even stronger. We rationalize this observation in terms of the almost uniform distribution of torsion angles the S–H bond makes with the aromatic plane in the precursor *p*-MePhSH in a room temperature solution, compared to the narrower distribution peaked around planarity found when the molecule is cooled in a molecular beam. This torsion coordinate is known to play a key role in channeling flux either on the diabat to ground ($\tilde{X}$) state products or to produce excited $\tilde{A}$ state products by remaining on the adiabatic surface. In ethanol, H-bonding interactions may provide a small bias in the torsional distribution towards planarity leading to relatively greater yields of $\tilde{X}$ state *p*-MePhS. The first pass branching ratio at longer photolysis wavelengths, where excitation is increasingly to S_1, is more even, at least for photodissociation in ethanol.

A second aspect highlighted in this work is our ability to consider the stereochemistry and mechanism for several different H + *p*-MePhS diffusive radical recombination pathways, in particular exploring the reactivity of the sulfur relative to the *o*- and *p*- ring carbon spin centers present in the two resonance forms of the *p*-MePhS radical. Although minor product channels, both *ortho*- (visible in both TA and UV-IR[25]) and *para*- (visible so far only in UV-IR experiments) recombination adducts are identified with the aid of ab initio computations.

Supporting Information: Steady state and time-resolved fluorescence methods and results; testing for photoproduct accumulation during TA experiments; ruling out contribution of coherent 2PA to support assignment for excited state *p*-MePhS radical; adduct IR band positions and intensities from *ab initio* calculations; kinetic models and target analysis for short-delay spectral fitting; additional data to support robustness of the pump-probe anisotropy recovered from experiment. This material is available free of charge *via* the Internet at http://pubs.acs.org.

Acknowledgements

The authors would like to thank Stephanie Harris and Daniel Murdock (University of Bristol) for valuable discussions. The work at USC is supported by the US National Science Foundation

under CHE-0957869 and at Bristol by the Engineering and Physical Sciences Research Council *via* Programme Grant EP/G00224X.

Figure 1

(a) UV absorption spectra for *p*-MePhSH in the vapor phase (black line), ethanol solution (orange line) and cyclohexane solution (blue line) between 310 > λ > 230 nm. The absorption intensities were normalized to the maxima at ~240 nm. (b) Expanded version of (a) between 250 > λ > 310 nm with the four Gaussian functions beneath representing the excitation pulses and their corresponding bandwidths. (c) Calculated CASPT2(10/10)/aug(S)-cc-pVTZ potential energy cuts through the S_0–S_3 and T_1–T_3 states in the S–H stretch dimension (the singlet states are reproduced from ref. 17) between 2.5 and 6.0 eV. Skeletal structures in (d) and (e) display transition dipole moments for *p*-MePhSH molecule, [17] and in (f) for the *p*-MePhS radical. [16]

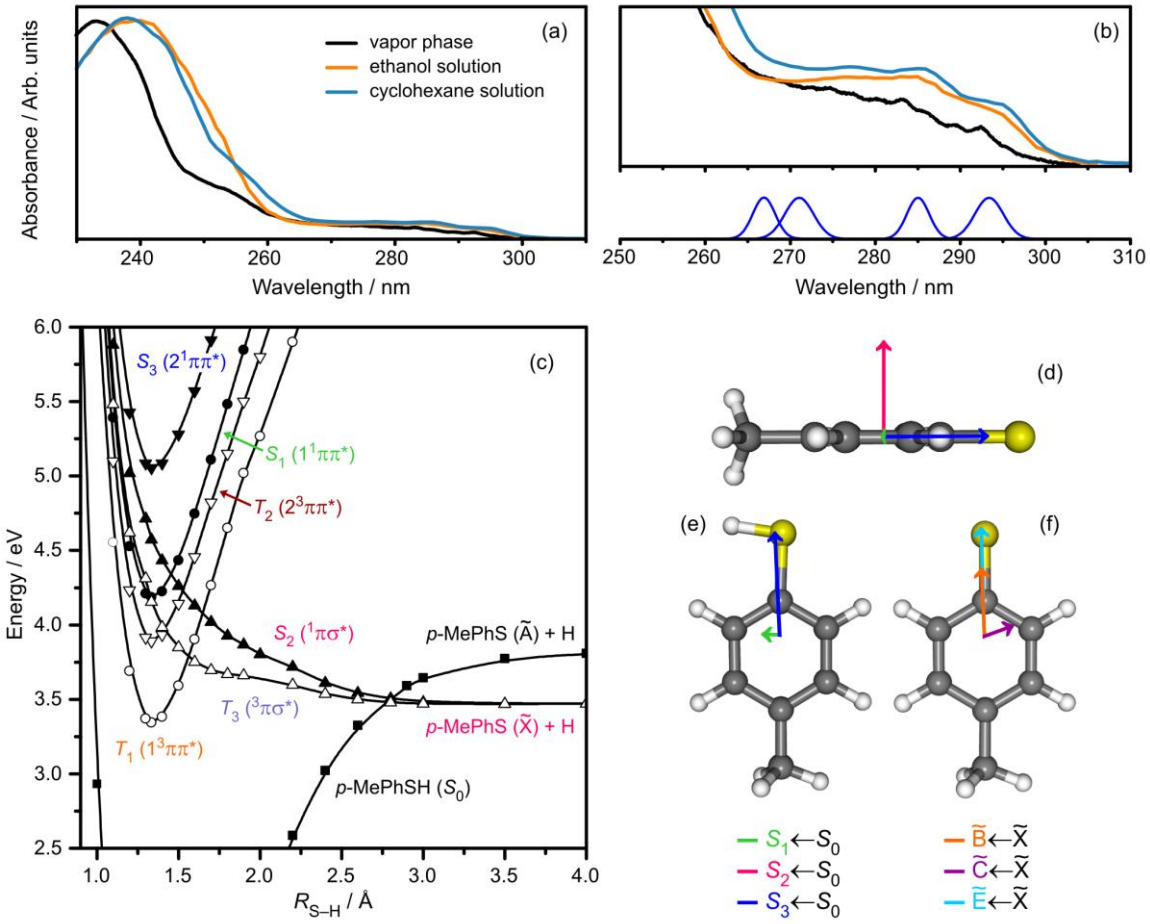

Figure 2

TA spectra of 90 mM *p*-MePhSH in ethanol for λ_{pump} = (a) 270 nm and (b) 295 nm at $0 \leq t \leq 200$ fs. The relative polarization between the pump and probe is set to magic angle. (c) Decay associated difference spectra and (d) time-dependent populations for each species from global analysis of the 270 nm pump dataset. S_1, *p*-MePhS $\tilde{X}$ and $\tilde{A}$ states as well as the notional initially excited S* are the species assumed in the target spectral analysis (see text) Calculated EOM-CCSD/aug-cc-pVTZ $S_n \leftarrow S_1$ ESA TDMs^2 from ref. 17 and CASSCF/aug-cc-pVTZ TDMs^2 for the *p*-MePhS radical product from ref. 16 are shown as colored bars at the foot of panels (a)-(c). The computed TDM^2 values for the $\tilde{X}$ and $\tilde{A}$ state radicals have been multiplied by factors of 10 and 100, respectively.

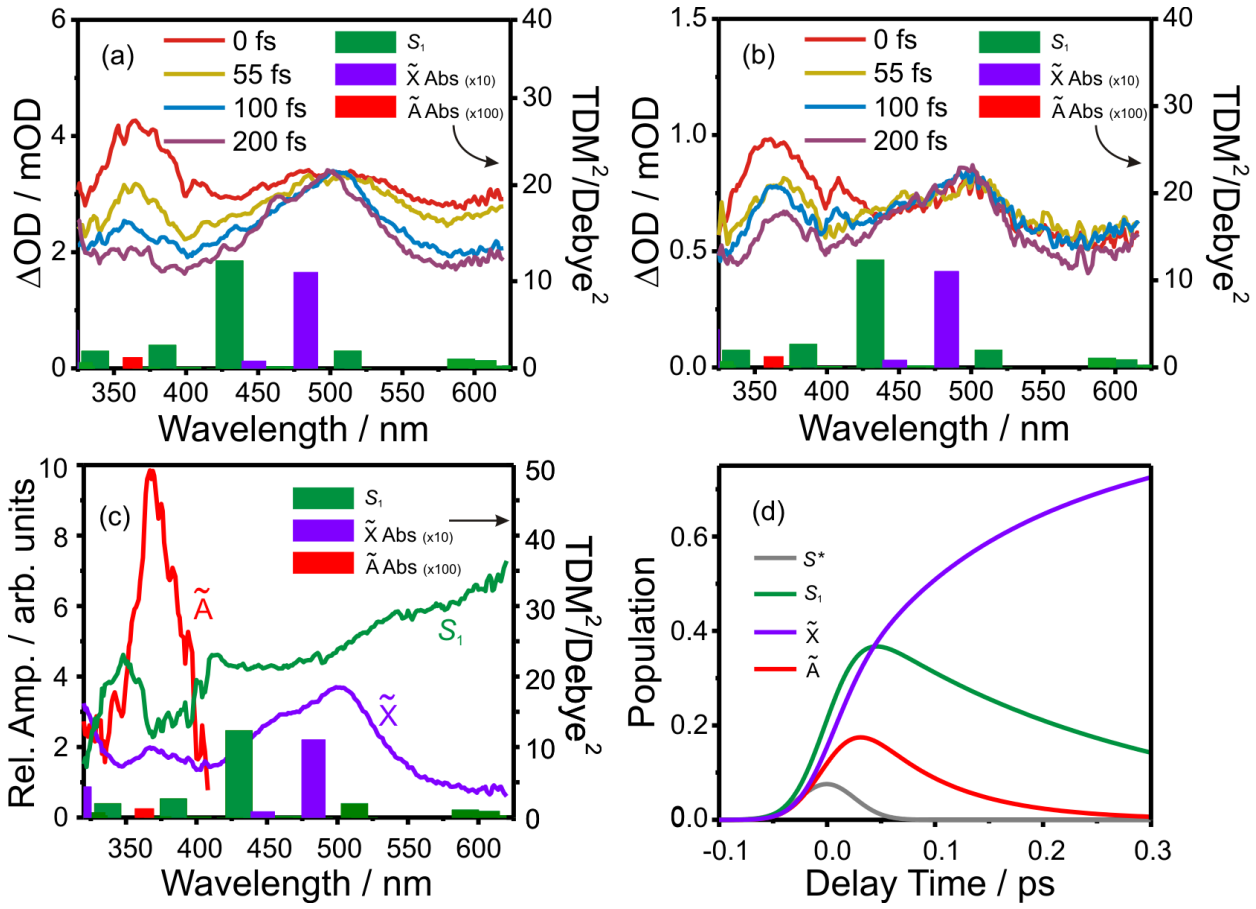

Figure 3

(a) TA spectra of 45 mM *p*-MePhSH in ethanol measured after 267 nm excitation at selected pump-probe delay times, with pump-probe polarization set to magic angle. (b) Time profiles of major TA features measured at λ_{probe} = 363, 500 and 600 nm. Inset: kinetics on an expanded scale, focusing on the early time.

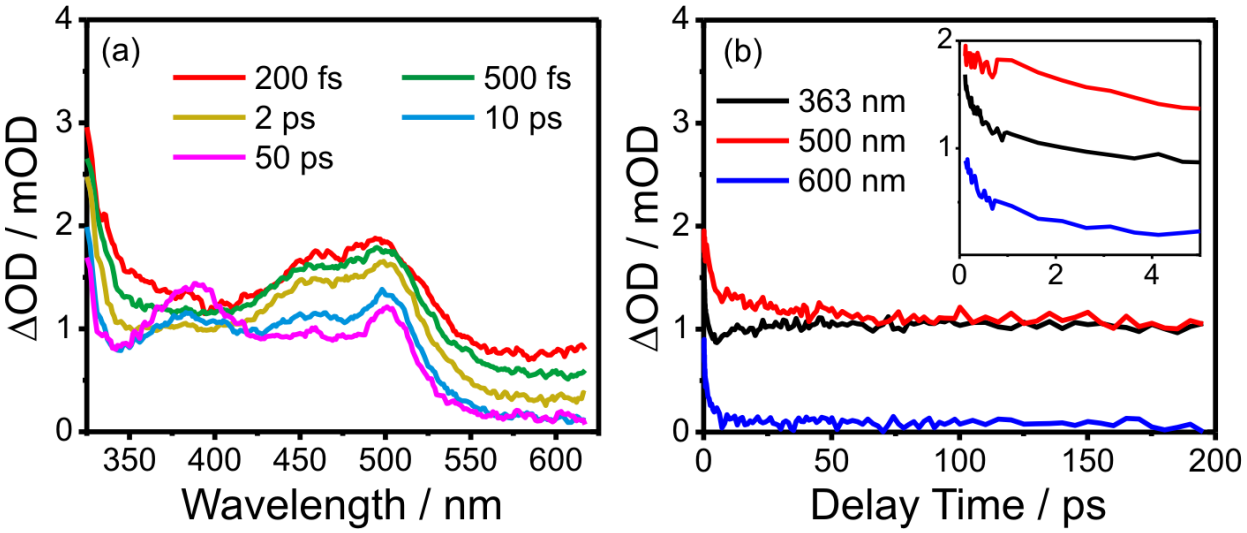

Figure 4

(a) TA spectra of 90 mM *p*-MePhSH in ethanol measured after 285 nm excitation at selected pump-probe delay times, with pump-probe polarization set to magic angle. (b) Time profiles of major TA features measured at λ_{probe} = 363, 500 and 600 nm. Inset: kinetics on an expanded scale, focusing on the early time.

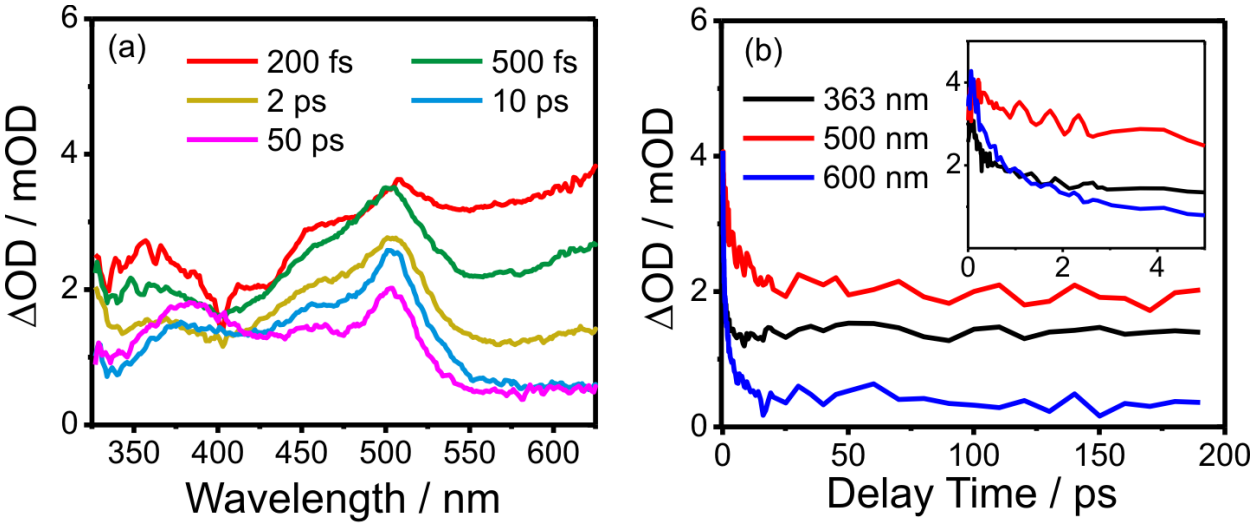

Figure 5

(a) TA spectra of 90 mM *p*-MePhSH in ethanol measured after 295 nm excitation at selected pump-probe delay times, with pump-probe polarization set to magic angle. The spectra were averaged over five delay time points to increase the signal-to-noise ratio. (b) Time profiles of major TA features measured at λ_{probe} = 363, 500 and 600 nm. Inset: kinetics on an expanded scale, focusing on the early time.

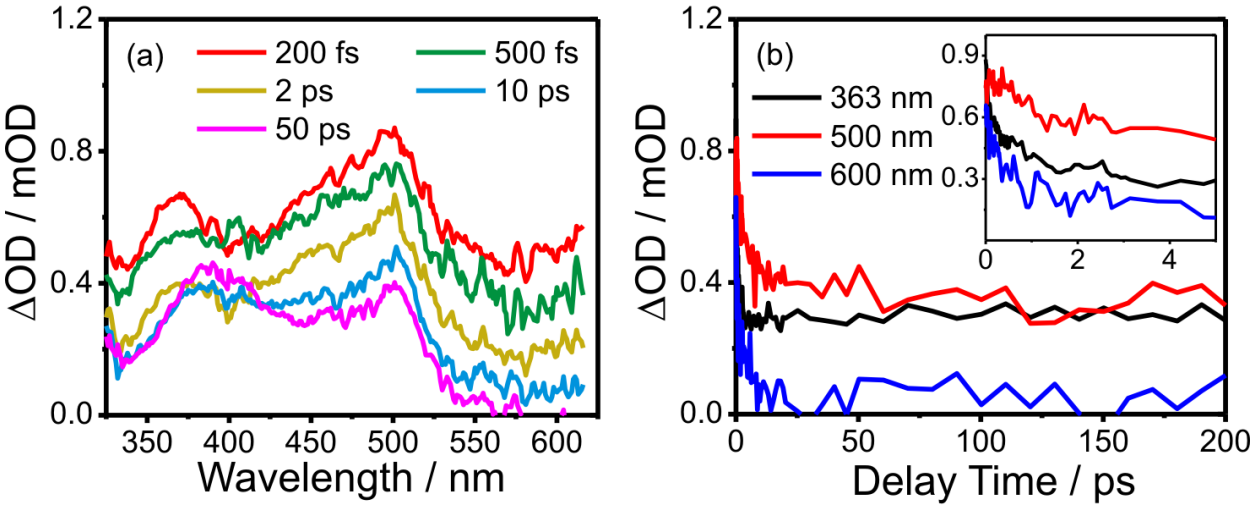

Figure 6

(a) Anisotropy spectra at early delay time (200 fs), obtained from sequential parallel and perpendicular polarization experiments. Regions associated with the $\tilde{X}$ and $\tilde{A}$ state *p*-MePhS radicals are shaded. (b) Anisotropy decay for *p*-MePhS($\tilde{X}$) radical band centered at 500 nm, obtained from simultaneous parallel and perpendicular polarization experiments utilizing the Wollaston prism. The traces obtained using 270 nm excitation are not shown since, within experimental error, they are identical to those from 267 nm excitation.

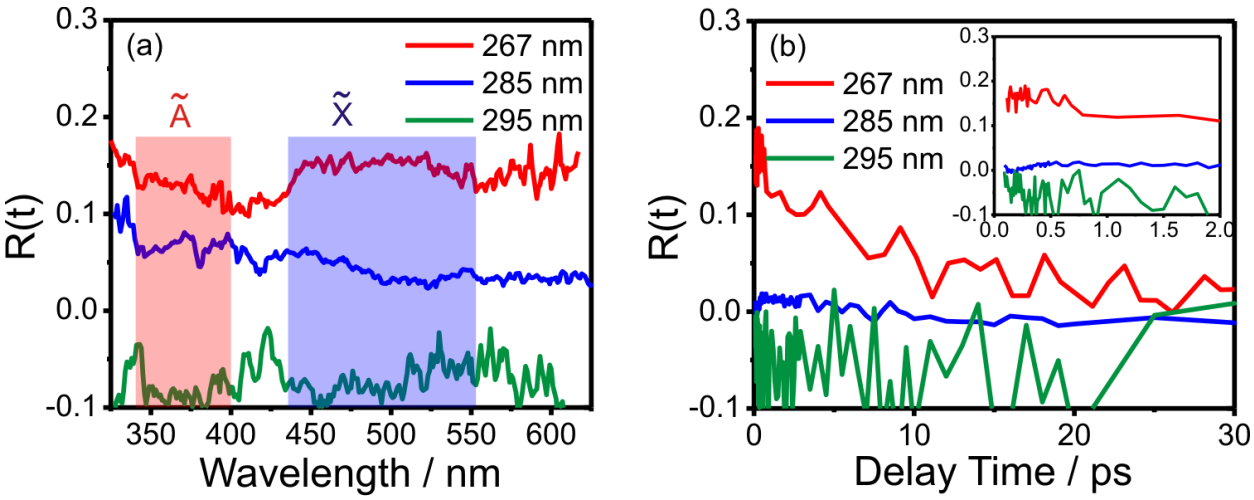

Figure 7

MP2/aug-cc-pVTZ optimized structures of the three possible adducts: A, B and C. The ground state energies are given relative to the absolute energy of the *p*-MePhSH molecule. [15] Ground state energies are calculated at the MP2//CCSD(T)-F12/aug-cc-pVTZ level, vertical excitation energies and associated TDM^2/ Debye^2 are from EOM-CCSD/aug-cc-pVTZ calculations.

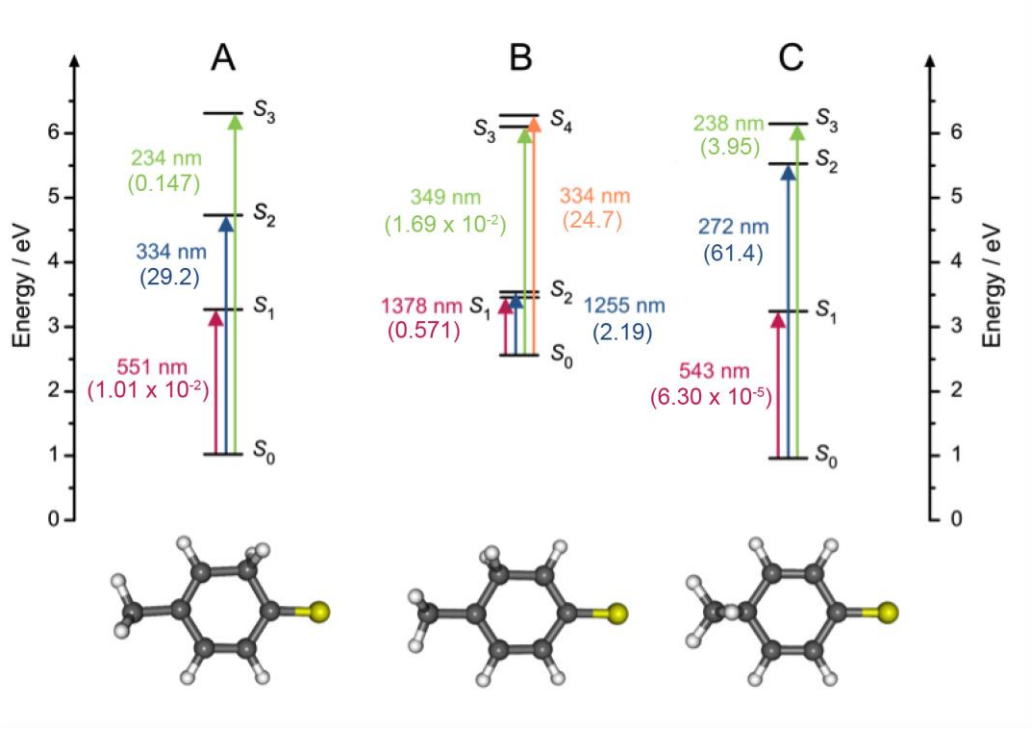

Figure 8

TA spectra of *p*-MePhSH in (a) ethanol and (b) cyclohexane at $0 \leq t \leq 200$ fs, excited with 270 nm and probed by broadband white light super-continuum pulses. The relative polarization of the pump and probe was set to = 54.7°.

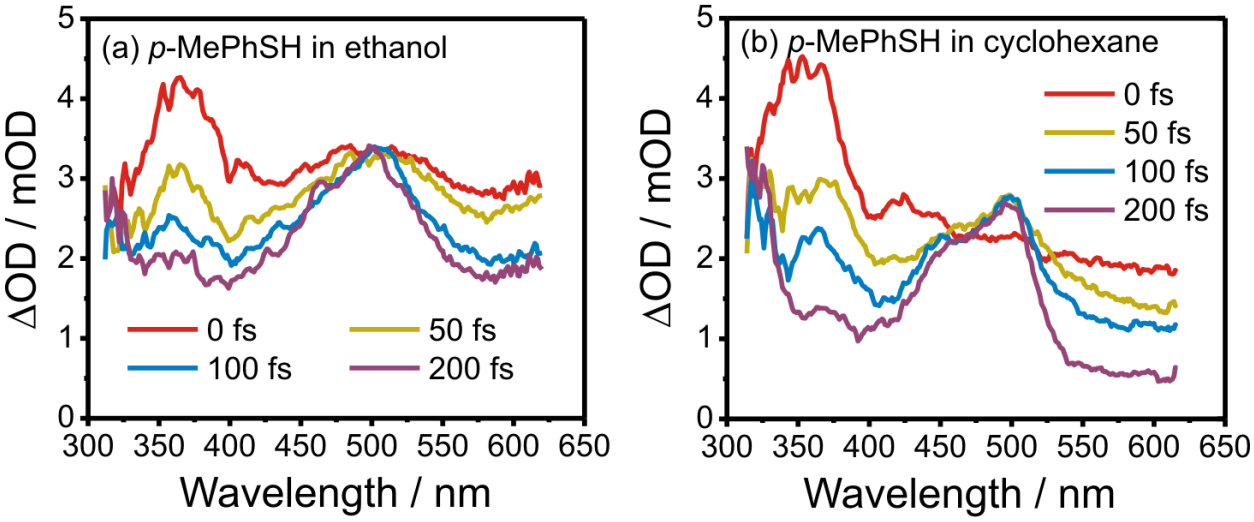

TOC Figure

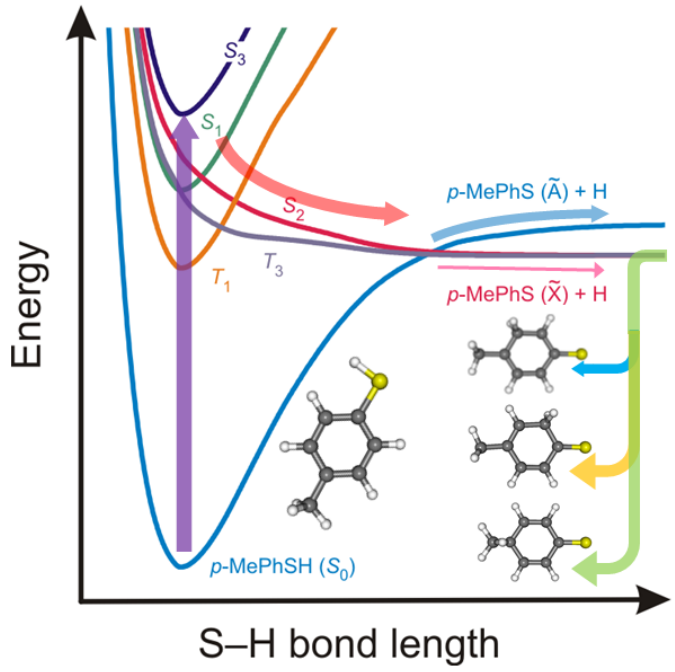
Energy
S–H bond length
S_3
S_1
S_2
T_1
T_3
p-MePhS (Ã) + H
p-MePhS (X̃) + H
p-MePhSH (S_0)

Notes and References

[1] Sobolewski, A. L.; Domcke, W.; Dedonder-Lardeux, C.; Jouvet, Excited-State Hydrogen Detachment and Hydrogen Transfer Driven by Repulsive $^1\pi\sigma^*$ states: A New Paradigm for Nonradiative Decay in Aromatic Biomolecules. C. *Phys. Chem. Chem. Phys.* **2002,** *4*, 1093-1100.

[2] Ashfold, M.N.R.; Cronin, B.; Devine, A.L.; Dixon, R.N.; Nix, M. G. D. The Role of $\pi\sigma^*$ Excited States in the Photodissociation of Heteroaromatic Molecule. *Science* **2006,** *312*, 1637-1640.

[3] Ashfold, M.N.R.; King, G.A.; Murdock, D.; Nix, M.G.D.; Oliver, T.A.A.; Sage, A. G. $\pi\sigma^*$ Excited States in Molecular Photochemistry. *Phys. Chem. Chem. Phys.* **2010,** *12*, 1218-1238, and references therein.

[4] Engel, V.; Staemmler, V.; Vanderwal, R.L.; Crim, F.F.; Sension, R.J.; Hudson, B.; Andresen, P.; Hennig, S.; Weide, K.; Schinke, R. Photodissociation of Water in the First Absorption Band: A Prototype for Dissociation on a Repulsive Potential Energy Surface. *J. Phys. Chem.* **1992** *96* 3201-3213.

[5] Mordaunt, D.H.; Ashfold, Dixon, R.N. Photodissociation Dynamics of $\tilde{A}$ State Ammonia Molecules. I. State Dependent μ-*v* Correlations in the $NH_2(ND_2)$ Products. M.N.R. *J. Chem. Phys.* **1996**, *104*, 6460-6471.

[6] Bach, A.; Hutchison, J.M.; Holiday, R.J.; Crim. F.F. Vibrational Spectroscopy and Photodissociation of Jet-Cooled Ammonia. *J. Chem. Phys.* **2002**, *116*, 4955-4961.

[7] Wen, Y.; Segall, J.; Dulligan, M.; Wittig, C. Photodissociation of Methanol at 193.3 nm: Translational Energy Release Spectra. *J. Chem. Phys.* **1994.** *101*, 5665-5671.

[8] Voth, G.A.; Hochstrasser, R.M. Transition State Dynamics and Relaxation Processes in Solutions: A Frontier of Physical Chemistry. *J. Phys. Chem.***1996**, *100*, 13034-13049.

[9] Winter, N.; Benjamin, I. Photodissociation of ICN at the Liquid/Vapor Interface of Water. *J. Chem. Phys.* **2004**, *121* 2253.

[10] Nadler, I.; Mahgerefteh, D.; Reisler H.; Wittig, C. The 266 nm Photolysis of ICN: Recoil Velocity Anisotropies and Nascent E,V,R,T Excitations for the CN+I($^2P_{3/2}$) and CN+I($^2P_{1/2}$) Channels. *J. Chem. Phys.* **1985**, *82*, 3885-3893.

[11] Rivera, C.A.; Winter, N.; Harper, R.V.; Benjamin, I.; Bradforth, S.E. The Dynamical Role of Solvent on the ICN Photodissociation Reaction: Connecting Experimental Observables Directly with Molecular Dynamics Simulations. *Phys. Chem. Chem. Phys.* **2011** 13, 8269-8283.

[12] Larsen, J.; Madsen, D.; Poulsen, J.A.; Poulsen, T.D.; Keiding, S.R.; Thøgersen, J. The Photoisomerization of Aqueous ICN Studied by Subpicosecond Transient Absorption Spectroscopy. *J. Chem. Phys.* **2002**, *116*, 7997-8005.

[13] Madsen, A.; Thomsen, C. L.; Poulsen, J. A.; Jensen, S. J. K.; Thøgersen, J.; Keiding, S. R.; Krissinel, E. B. Femtosecond Photolysis of HOCl(aq): Dissipation of Fragment Kinetic Energy. *J. Phys. Chem. A* **2003**, *107*, 3606-3611.

[14] Thomsen, C.L.; Philpott, M.P.P.; Hayes, S.C.; Reid, P.J. The Formation of ClOO Following the Photoexcitation of Aqueous OClO Studied by Two-color, Time-Resolved Resonance Raman Spectroscopy. *J. Chem. Phys.* **2000**, *112*, 505-508.

[15] Oliver, T.A.A.; King, G.A.; Tew, D.P.; Dixon R.N.; Ashfold, M.N.R. *J. Phys. Chem. A* Controlling Electronic Product Branching at Conical Intersections in the UV Photolysis of *para*-Substituted Thiophenols. **2012**, *116* 12444-12459.

[16] Oliver, T.A.A.; Zhang, Y.; Ashfold, M.N.R.; Bradforth, S.E. Linking Photochemistry in the Gas and Solution Phase: S–H Bond Fission in *p*-Methylthiophenol Following UV Photoexcitation. *Faraday Discuss.* **2011**, *150*, 439-458.

[17] Zhang, Y.; Oliver, T.A.A.; Ashfold, M.N.R.; Bradforth, S.E. Contrasting the Excited State Reaction Pathways of Phenol and *para*-Methylthiophenol in the Gas and Liquid Phase. *Faraday Discuss.* **2012**, *157*, 141-163.

[18] Reichardt, C.; Guo, C.; Crespo-Hernández, C. Excited-State Dynamics in 6-Thioguanosine from the Femtosecond to Microsecond Time Scale. *J. Phys. Chem. B* **2011**, *115*, 3263-3270

[19] Pecourt, J. M. L.; Peon, J.; Kohler, B., Ultrafast Internal Conversion of Electronically Excited RNA and DNA Nucleosides in Water. *J. Am. Chem. Soc.* **2000,** 122, 9348-9349

[20] Lim, J.S.; Lim, I.S.; Lee, K.S.; Ahn, D.S.; Lee Y.S.; Kim, S.K. Intramolecular Orbital Alignment Observed in the Photodissociation of [D_1]Thiophenol. *Angew. Chem. Int. Ed.* **2006**, *45*, 6290-6293.

[21] Devine, A.L.; Nix, M.G.D.; Dixon R.N.; Ashfold, M.N.R. Near-Ultraviolet Photodissociation of Thiophenol. *J. Phys. Chem. A* **2008**, *112*, 9563-9574.

[22] Venkatesan, T.S.; Ramesh, S.G.; Lan Z.; Domcke, W. Theoretical Analysis of Photoinduced H-Atom Elimination in Thiophenol. *J. Chem. Phys.*, **2012**, *136*, 174312-16.

[23] Pino, G.A.; Oldani, A. N.; Marceca, E.; Fujii, M.; Ishiuchi, S. I.; Miyazaki, M.; Broquier, M.; Dedonder C.; Jouvet, C. Excited State Hydrogen Transfer Dynamics in Substituted Phenols and Their Complexes with Ammonia: $\pi\pi^*$-$\pi\sigma^*$ Energy Gap Propensity and *Ortho*-Substitution Effect. *J. Chem. Phys.* **2010**, *133*, 124313-12.

[24] Dixon, R.N.; Oliver T.A.A.; Ashfold, M.N.R. Tunneling Under a Conical Intersection: Application to the Product Vibrational State Distributions in the UV Photodissociation of Phenols. *J. Chem. Phys.* **2011**, *134*, 194303-10.

[25] Murdock, D.; Harris, S.J.; Karsili, T.N.V.; Greetham, G.M.; Clark, I.P.; Towrie, M.; Orr-Ewing, A.J.; Ashfold, M.N.R. Photofragmentation Dynamics in Solution Probed by Transient IR Absorption

Spectroscopy: πσ*-Mediated Bond Cleavage in *p*-Methylthiophenol and *p*-Methylthioanisole. *J. Phys. Chem. Lett.* **2012**, 3, 3715-3720.

[26] Harris, S.J.; Murdock, D.; Zhang, Y.; Oliver, T.A.A.; Grubb, M.P.; Orr-Ewing, A.J.; Greetham, G.M.; Clark, I.P.; Towrie, Bradforth, S.E. *et al.* Comparing Molecular Photofragmentation Dynamics in the Gas and Liquid Phases. *Phys. Chem. Chem. Phys.* **2013**, 15, 6567-6582.

[27] Kloepfer, J. A.; Vilchiz, V. H.; Lenchenkov, V. A.; Germaine, A. C.; Bradforth, S. E., The Ejection Distribution of Solvated Electrons Generated by the One-Photon Photodetachment of Aqueous I^- and Two-Photon Ionization of the Solvent. *J. Chem. Phys.* **2000,** 113, 6288-6307.

[28] Rivera, C.A.; Bradforth S.E.; Tempea, G. Gires-Tournois Interferometer Type Negative Dispersion Mirrors for Deep Ultraviolet Pulse Compression. *Opt. Express* **2010**, *18*, 18615-18624.

[29] Tauber, M.J.; Mathies, R.A.; Chen X.Y.; Bradforth, S. E. Flowing Liquid Sample Jet for Resonance Raman and Ultrafast Optical Spectroscopy. *Rev. Sci. Instrum.* **2003**, *74*, 4958-4960.

[30] MOLPRO is a package of *ab initio* programs written by Werner, H.-J.; Knowles, P.J.; Manby, F.R.; Schütz, M.; Celani, P.; Knizia, G.; Korona, T.; Lindh, R.; Mitrushenkov, A.; Rauhut, G.; Adler, T.B.; *et al.* Cardiff, **2010**.

[31] To avoid any potential confusion throughout the manuscript, we refer to the diabatic S_1–S_3 states according to their ordering in the vFC region.

[32] Elles, C.G.; Rivera, C.; Zhang, Y.; Pieniazek, P.A.; Bradforth, S.E. Electronic Structure of Liquid Water from Polarization-Dependent Two-Photon Absorption Spectroscopy. *J. Chem. Phys.* **2009** *130*, 084501-13.

[33] Zhang, Y. Two-photon Absorption Spectroscopy and Excited State Photochemistry of Small Molecules. PhD thesis, **2012**, University of Southern California.

[34] Thyrion, F.C. Flash Photolysis of Aromatic Sulfur Molecules. *J. Phys. Chem.* **1973**, *77*, 1478-1482.

[35] Tripathi, G.N.R.; Sun, Q.; Armstrong, D.A.; Chipman, D.M.; Schuler, R.H. Resonance Raman Spectra and Structure of Phenylthiyl Radical. *J. Phys. Chem.* **1992**, *96*, 5344-5350.

[36] Hermann, R.; Dey, G.R.; Naumov S.; Brede, O. Thiol Radical Cations and Thiyl Radicals as Direct Products of the Free Electron Transfer From Aromatic Thiols to *n*-Butyl Chloride Radical Cations. *Phys. Chem. Chem. Phys.* **2000**, *2*, 1213-1220.

[37] Stokkum, I. van ; Larsen, D. S.; Grondelle, R. van; Global and Target Analysis of Time-Resolved Spectra. *Biochem. Biophys. Acta* **2004**, *1657*, 82-104.

[38] Riyad, Y.M.; Naumov, S.; Hermann R.; Brede, O. Deactivation of the First Excited Singlet State of Thiophenols. *Phys. Chem. Chem. Phys.* **2006**, *8*, 1697-1706.

[39] Chen, X.Y.; Larsen, D.S.; Bradforth S.E.; van Stokkum, I.H.M. Broadband Spectral Probing Revealing Ultrafast Photochemical Branching after Ultraviolet Excitation of the Aqueous Phenolate Anion. *J. Phys. Chem. A* **2011**, *115*, 3807-3819.

[40] Jha, K.N.; Bolton G.L.; Freeman, G.R. Temperature shifts in the optical spectra of solvated electrons in methanol and ethanol. *J. Phys. Chem.* **1976**, *76*, 3876-3883.

[41] Silva, C.; Walhout, P.K.; Reid, P.J.; Barbara, P.F. Detailed Investigations of the Pump-Probe Spectroscopy of the Equilibrated Solvated Electron in Alcohols. *J. Phys. Chem. A* 1998, *102*, 5701-5707.

[42] Elles, C.G.; Shkrob, I.A.; Crowell R.A.; Bradforth, S.E. Excited state dynamics of liquid water: Insight from the dissociation reaction following two-photon excitation. *J. Chem. Phys.* **2007**, *126*, 164503-8.

[43] Thomsen, C.L.; Madsen, D.; Poulsen, J.A.; Thøgersen, J.; Knack Jensen, S.J.; Keding, S.R. Femtosecond photolysis of aqueous HOCl. *J. Chem. Phys.* **2001**, *115*, 9361-9370.

[44] Seidel, R.; Winter B.; Bradforth, S. E. *unpublished results*.

[45] Faulk, J. D.; Dunbar, R. C.; Lifshitz, C. Slow Dissociations of Thiophenol Molecular Ion. Study by TRPD and TPIMS (Time-Resolved, Photodissociation and Time-Resolved Photoionization Mass Spectrometry). *J. Am. Chem. Soc.* **1990**, *112*, 7893−7899.

[46] Reisler, H.; Krylov, A. Interacting Rydberg and Valence States in Radicals and Molecules: Experimental and Theoretical Studies. *Int. Rev. Phys. Chem.* **2009**, *28*, 267-308.

[47] Bradforth, S.E. General Discussion. *Faraday Discuss.* **2011**, *150*, 505-532.

[48] Oliver, T.A.A; Ashfold, M.N.R., *Unpublished data.*

[49] Sarangi, R.; Frank, P.; Benfatto, M.; Morante, S.; Minicozzi, V.; Hedman, B.; Hodgson, K.O. The X-Ray Absorption Spectroscopy Model of Solvation about Sulfur in Aqueous L-Cysteine. *J. Chem. Phys.* **2012**, *137*, 205103-20.

[50] The same equation was used to fit the geminate recombination between *p*-MePhS radical and the hydrogen atom in Refs. 9 and 10, but a typographical error was found in these two references: the term "t_0" in the equation should in fact be "t_g" as shown correctly in the current article.

[51] Elles, C.G.; Jailaubekov, A.E.; Crowell, R.A.; Bradforth, S.E. Excitation-energy dependence of the mechanism for two-photon ionization of liquid H_2O and D_2O from 8.3 to 12.4 eV. *J. Chem. Phys.* **2006**, *125* 04415-12.

[52] CRC Handbook of Chemistry and Physics. 91st ed., Taylor and Francis**,** USA,2009.

[53] Ichino, T. On the Mechanism of Unusual CIDEP. PhD thesis, **2001**, University of Notre Dame.